THE JOURNAL OF PHYSICAL CHEMISTRY C
A JOURNAL OF THE AMERICAN CHEMICAL SOCIETY

pubs.acs.org/JPCC

Article

Multifunctional 4,5-Diphenyl-1*H*-imidazole-Based Luminogens as Near UV/Deep Blue Emitters/Hosts for Organic Light-Emitting Diodes and Selective Picric Acid Detection

Published as part of The Journal of Physical Chemistry virtual special issue "Early-Career and Emerging Researchers in Physical Chemistry Volume 2".

Sandhya Rani Nayak, Shahnawaz, Iram Siddiqui, Jwo-Huei Jou, Sabita Patel, and Sivakumar Vaidyanathan*

Cite This: *J. Phys. Chem. C* 2023, 127, 499−515

Read Online

ACCESS | Metrics & More | Article Recommendations | Supporting Information

ABSTRACT: A series of luminophores (construction of diphenylimidazole (m-CF_3PTPI) groups functionalized at the N1-positions of imidazole groups) were purposefully designed and synthesized for optoelectronics and for selective detection of nitroaromatic compounds. The luminophores showed deep blue emission in solution, solid, and thin-film matrix with acceptable quantum yield and good thermal stability (5% weight loss at 258−296 °C). From electrochemical analysis as well as theoretical calculations, the energy gaps of HOMO−LUMO are found to be in good agreement and all of them showed good triplet energy. The luminophores can be explored as hosts for phosphorescent organic light-emitting diodes (PhOLEDs). Furthermore, the m-CF_3PTPI derivatives were used as emitters for fluorescent OLEDs and hosts (m-CF_3PTPI-1 and m-CF_3PTPI-2) for triplet dopants in PhOLEDs. Near-UV emissions were observed for all the doped devices that exhibited electroluminescence (EL) peaks at ∼380−395 nm with a Commission International deL'Eclairage (CIE_y) coordinate of ∼0.09. Of all the devices, the m-CF_3PTPI-5 (3 wt %)-based device demonstrated a maximum external quantum efficiency (EQE_{max}) of 2.8%, power efficiency (PE_{max}) of 0.9 lm/W, current efficiency (CE_{max}) of 1.3 cd/A, and brightness of 953 cd/m^2. Moreover, the device was further optimized using a different host approach. SimCP2 displayed the best performance by achieving a high EQE_{max} of 4.0% that is near the theoretical limit of fluorescent materials. Furthermore, m-CF_3PTPI-1 and m-CF_3PTPI-2 possessing triplet energies of 2.67 and 2.63 eV, respectively, were used as hosts for efficient green ($Ir(ppy)_3$-2.4 eV) PhOLEDs. The m-CF_3PTPI-2-based device achieved an EQE_{max} of 4.8%, CE_{max} of 17.5 cd/A, PE_{max} of 13.4 lm/W, and maximum brightness (L_{max}) of 4695 cd/m^2, much higher than those of the counterpart m-CF_3PTPI-1-based OLED. Furthermore, due to structural functionality, the detection of nitroaromatic compounds was carried out for all the luminophores. They showed high sensitivity toward picric acid, and the sensing mechanism was thoroughly analyzed by using NMR and DFT study.

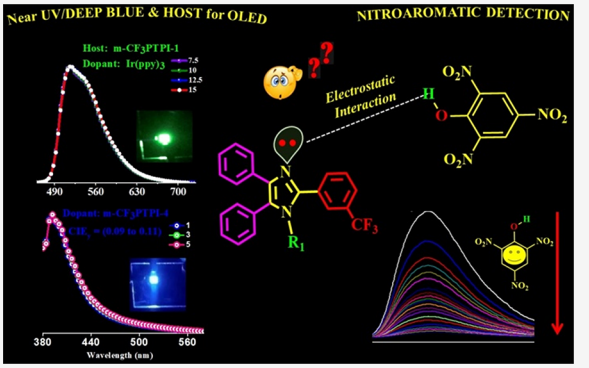

INTRODUCTION

Simple functional organic fluorophores have gained enormous attention due to their easy synthetic procedure and structure-dependent alteration, which impact the desired properties (optoelectronics, chemosensing, organic photovoltaics, etc.).[1,2] Owing to their unique features (lower energy consumption, cost-effectiveness, lightweight, and flexibility), organic light-emitting diodes (OLEDs) are considered as promising alternatives for smart displays and solid-state lightings.[3,4] In comparison with fluorescent emitters, metal-based phosphorescent dopants[5] as well as thermally activated delayed fluorescence (TADF) emitters have shown promising EQE (>5%) due to their ability to break through the spin statistics rules (to achieve near unity internal quantum efficiency (IQE)). However, preserving high efficiency at high brightness is an incredible task for several applications.[6,7] Also, it is worth noting that achieving widened color gamut, near UV/deep blue emitters with a CIE_y coordinate of <0.10 that even match the blue standard with the CIE (*x*, *y*) coordinates at (0.15, 0.06) of European Broadcasting Union (EBU) is crucial to full-

Received: July 24, 2022
Revised: November 26, 2022
Published: December 22, 2022

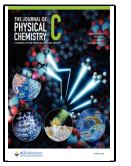

color displays. Thus, simultaneous realization of near UV/deep blue luminophores with high efficiency and color saturation CIE_y < 0.10 is a formidable challenge in high-performance display devices.[8,9] The use of precious metals (Ir, Pt, or Au) and the effect of strong self-quenching of long-lived triplet excitons at high luminescence restrict wider usage of PhOLEDs.[10,11] Both phosphorescent metal complexes and TADF-based emitters need to be doped in an appropriate host material to evade self-quenching. An ideal host should fulfill certain pre-requirements, such as high triplet energy, balanced carrier mobilities, and chemical and thermal robustness.[12,13] The use of traditional blue fluorescent materials as emitters and hosts gained still considerable attention for OLEDs.

Recently, many researchers give their great efforts to focus on designing small organic luminescent materials (unipolar) because of their ordered molecular structure, easy purification process, and flexibility in structural modification. An imidazole moiety is more recommended because of its high thermal stability and sensing ability.[14,15] The electron-deficient characteristics of imidazole makes the molecule highly polar, and the availability of a lone pair on imidazole nitrogen helps in sensing and allowing efficient electron transfer in devices. The unipolar TPI derivatives fabricated in a *N*,*N*′-dicarbazolyl-4,4′-biphenyl (CBP) host found OLED performances of 1.4% EQE with (0.23, 0.21) CIE coordinates in the blue region with good chemosensing behavior.[16] The BIPTPA-based device displayed EL performance with an L_{max} of 413 cdm^{-2}, EQE of 1.2%, and CE of 0.5 cdA^{-1} at 100 cdm^{-2} with a CIE of (0.16, 0.07), analogous to pure blue light.[17−19] Formation of controlled energy levels along with the ability to transfer electrons and holes, which has been presented simultaneously, can be achieved by the presence of reliable electron-rich and electron-deficient moieties in a molecular structure.[20] Therefore, to accomplish full color displays, simple organic fluorophores with near UV/deep blue emitters need to be designed.

As we are aware that the presence of different toxic pollutants such as explosive nitroaromatics compounds (phenol (PH), benzoic acid (BA), 4-nitrophenol (4-NP), 2,4-dinitrophenol (2,4-DNP), and picric acid (PA)) are dangerous for the environment and mankind, therefore, visualization and quick detection of such toxic pollutants are highly recommended.[21,22] Multifunctional luminophores can be widely used for detection of such toxic explosive compounds from the environment and behave as excellent chemosensors.[23,24] Taking advantage of the availability of lone pairs in nitrogen, it could be a possible candidate for nitroaromatic compound detection. Keeping this in mind, a series of unipolar simple organic fluorophores were designed and synthesized. Diphenylimidazole-based luminophores (m-CF_3PTPI) are found to be the best class of molecular core as their properties can be tuned by functionalizing at either N1 or C1 positions. Therefore, in the present investigation, the diphenylimidazole core is functionalized because of its good thermal stability as well good charge transporting properties with different substituents (electron-withdrawing groups (EWG) and electron-donating groups (EDG)) at the N1 position (the availability of a nitrogen lone pair for chemosensing as well as influence on photophysical properties simultaneously used for the OLED application, which shows a good EQE), keeping the C1 position fixed, as shown in Figures 1 and 2. Correlated with their nonfluorinated counterparts, fluorinated fluorophores display low-lying energy levels in both

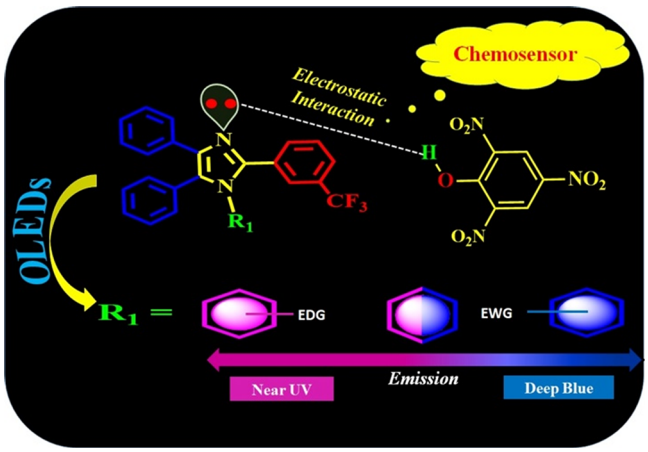

Figure 1. Design strategy of luminophores (EWG/EDG combination).

the LUMO and HOMO without severe disruption in the bandgap. Among strong EWGs such as sulfonyl (SO_2), cyano (CN), and trifluoromethyl (CF_3), particularly, the *m*-CF_3 moiety has garnered considerable interest because it not only acquires a higher electron-withdrawing capability but also facilitates facile adjustment of imperative properties including solubility and thermal and chemical stability.[25] So, we made an attempt by keeping the C1 position with an electron-withdrawing group (m-CF_3) to increase the mobility of electrons and balancing the charge in the device as well as lowering the bandgap, which ultimately enhance the device performance and also help in tuning the PL spectra.[26−28] Also, the higher electron-withdrawing capability of CF_3 can make it more benign for lowering the level of HOMO energy. Owing to the important contribution of *m*-CF_3 in the fluorophores, a noticeable change in optical and electrochemical properties together with a significant increment in OLED device performance is revealed.

Remarkably, all m-CF_3PTPI derivatives showed near UV/deep blue emission in solution, solid, and thin film. The synthetic route was designed by a simple one-pot condensation method in which the starting materials are easily available. These luminophores are explored as a possible near UV/deep blue emitter as well as a host for green PhOLEDs. In addition, these luminophores showed noble selectivity for picric acid (PA) over other explosive compounds such as PH, BA, 4-NP, and 2,4-DNP. It is worth noting that among all, m-CF_3PTPI-2 luminophores showed high sensitivity as well as good selectivity for PA detection. It is well documented that the presence of a nitrogen atom on luminophores makes them more basic, and it can strongly bind with acidic PA that leads to fluorescence (emission) quenching and shown chemosensing behavior. The luminophores contain an electron-donating methyl group, which makes the lone pair on the nitrogen atom more available, which enhances the interaction with PA as compared to other EWGs present at the N1-position of phenyl rings. It is evident that the detection limit (DL) of the luminophores containing EDGs is highly promising.

As mentioned earlier, the synthesized luminophores were explored for OLED application as near UV/deep blue emitters or host materials for PhOLEDs. Furthermore, the electronic and optical characteristics of charge transporting materials have been thoroughly investigated to obtain a detailed under-

https://doi.org/10.1021/acs.jpcc.2c05220
J. Phys. Chem. C 2023, 127, 499−515

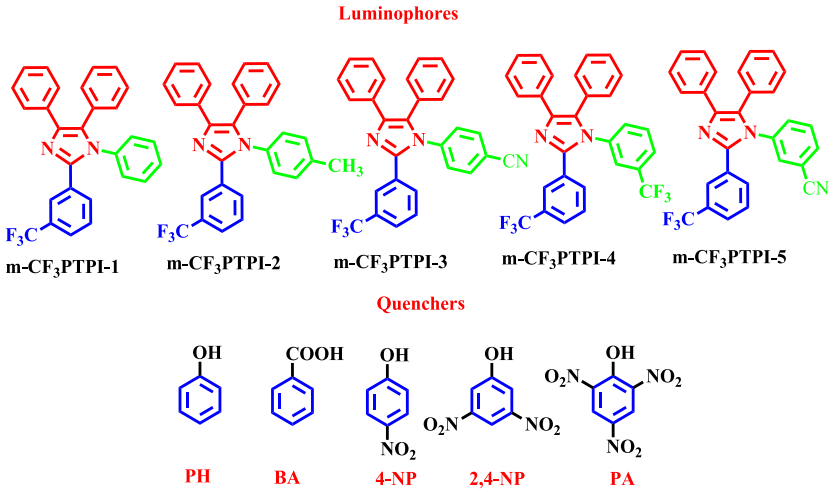

Figure 2. Structures of imidazole-based luminophores (top) and quenchers (down) used for chemosensors.

standing. In addition, the effect of substitution on the fluorophores and their quantum chemical studies have also been discussed. According to the theoretical calculation of m-CF_3PTPI-based luminophores, we carry forward the development of potential near UV/deep-blue emitters.

To achieve efficient OLED devices, the correlation between electroluminescence (EL) performances and substituent groups on the luminophores was also examined. We fabricated imidazole-based materials as blue emitters with host CBP for blue OLED devices via a solution process. Among the five imidazole-based materials, two materials (m-CF_3PTPI-1 and m-CF_3PTPI-2) having high triplet energy and suitable HOMO/LOMO were employed as hosts for the green PhOLED. The device configurations for blue and green OLEDs are ITO/PEDOT:PSS/CBP:luminophores (x wt %)/TPBi/LiF/Al and ITO/PEDOT:PSS/m-CF_3PTPI-1 or m-CF_3PTPI-2:$Ir(ppy)_3$/TPBi/LiF/Al, respectively. The EL performances were investigated, and among all the blue emitters, the device incorporated with m-CF_3PTPI-5 (3 wt %) achieved the highest performance with a maximum PE_{max} of 0.9 lm/W, CE_{max} of 1.3 cd/A, and EQE_{max} of 2.8% at a brightness of 953 cd/m^2. Meanwhile, in the case of green OLEDs, devices based on host m-CF_3PTPI-2 doped with green dye ($Ir(ppy)_3$) (12.5 wt %) displayed a CE_{max} of 17.5 cd/A, PE_{max} 13.4 lm/W, EQE_{max} of 4.8%, and L_{max} of 4695 cd/m^2 comparative to the m-CF_3PTPI-1-based device.

EXPERIMENTAL DETAILS

Synthesis. Benzil, 3-(trifluoromethyl)-benzaldehyde, an equivalent amount of amine derivative, along with ammonium acetate (NH_4OAc) was dissolved in glacial acetic acid (CH_3COOH) (25 mL) at 120 °C and kept overnight, as shown in Scheme 1. The resulting mixture was poured in ice water, and an organic layer was extracted with DCM. The crude product was made by adding a silica gel to the extracted product. The crude was purified by column chromatography (silica gel) eluted with a mixture of ethyl acetate/petroleum ether (3:7; v/v) to give a white-colored solid compound. Structurally, luminophores were confirmed by spectroscopic methods, i.e., ^{1}H, ^{13}C NMR, and HRMS spectrometry, as displayed in Figures S2 to S16 (Supporting Information).

1,4,5-Triphenyl-2-(3-(trifluoromethyl)phenyl)-1H-imidazole (m-CF_3PTPI-1). Yield: 75%, white solid, melting point = 130.8 °C, ^{1}H NMR (400 MHz, $CDCl_3$, δ ppm): 7.72 (s, 1H), 7.67−7.60 (m, 3H), 7.53 (d, J = 7.8 Hz, 1H), 7.41−7.20 (m, 10H), 7.20−7.15 (m, 2H), 7.12−7.06 (m, 2H). ^{13}C NMR (100 MHz, $CDCl_3$, TMS, δ ppm): 145.47 (s), 136.70 (s), 134.14 (s), 131.83 (s), 131.23 (s), 131.08 (s), 130.26 (s), 129.35 (s), 128.70 (s), 128.59 (s), 128.44 (s), 128.34 (s), 128.27 (s), 128.18 (s), 127.45 (s), 127.38 (s), 126.84 (s), 125.73 (q, J = 3.9 Hz), 125.21 (s), 124.70 (q, J = 3.7 Hz), 122.50 (s), 77.30 (d, J = 11.4 Hz), 77.04 (s), 76.72 (s). EI-MS: m/z exp. (calc.) 440.1500 found 441.1573 $[M + H]^+$.

Scheme 1. Synthetic Procedure of the m-CF_3PTPI Imidazole-Based Luminophores

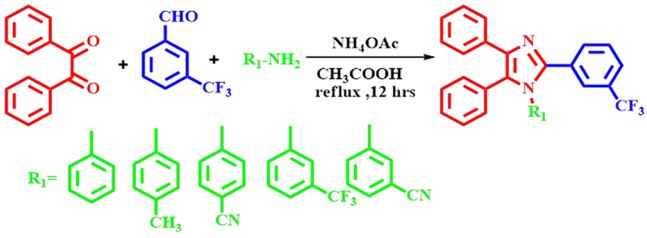

4,5-Diphenyl-1-(p-tolyl)-2-(3-(trifluoromethyl)phenyl)-1H-imidazole (m-CF_3PTPI-2). Yield: 80%, white solid, melting point = 175.3 °C, ^{1}H NMR (400 MHz, $CDCl_3$, TMS, δ ppm): 2.35 (3H, s), 6.95−6.96 (2H, d, J = 8 Hz), 7.09−7.11 (2H, d, J = 8.4 Hz), 7.16−78 (2H, dd J = 2 Hz, 8 Hz), 7.23−7.30 (6H, m), 7.34−7.38 (1H, m), 7.51−7.53 (1H, d, J = 8 Hz), 7.60−7.62 (3H, d, J = 7.2 Hz), 7.74 (1H, s). ^{13}C NMR (100 MHz, $CDCl_3$, TMS, δ ppm) 145.37 (s), 138.67 (d, J = 18.4 Hz), 134.16 (d, J = 16.5 Hz), 131.78 (s), 131.44 (d, J = 17.6 Hz), 131.06 (d, J = 9.1 Hz), 130.69 (s), 130.38 (d, J = 2.6 Hz), 129.93 (s), 128.67−127.90 (m), 127.38 (s), 126.78 (s), 125.73 (q, J = 3.9 Hz), 124.70 (q, J = 3.7 Hz), 77.36 (s), 77.04 (s), 76.72 (s), 21.15 (s). EI-MS: m/z exp. (calc.) 454.1657 found 455.1732 $[M + H]^+$.

4-(4,5-Diphenyl-2-(3-(trifluoromethyl)phenyl)-1H-imidazol-1-yl)benzonitrile (m-CF_3PTPI-3). Yield: 80%, white solid, melting point = 193.0 °C, ^{1}H NMR (400 MHz, DMSO-d_6, TMS, δ ppm): 7.23−7.27 (1H, m), 7.31−7.34 (3H, m), 7.39−7.42 (2H, m), 7.45−7.49 (2H, m), 7.52−7.58 (5H, q), 7.73−7.74 (2H, d, J = 4 Hz), 8.38−8.40 (2H, m), 8.45 (1H, s). ^{13}C NMR (100 MHz, DMSO-d_6, TMS, δ ppm): 144.42 (s), 137.96 (s), 135.31 (s), 131.69 (s), 131.25 (s), 130.43 (s), 129.51−

https://doi.org/10.1021/acs.jpcc.2c05220
J. Phys. Chem. C 2023, 127, 499−515

129.09 (m), 128.82 (d, J = 18.7 Hz), 128.48 (s), 127.58 (s), 127.20 (s), 125.03 (dd, J = 7.5, 3.5 Hz), 121.88 (dd, J = 7.7, 4.0 Hz), 40.60 (s), 40.39 (s), 40.19 (s), 39.98 (s), 39.77 (s), 39.56 (s), 39.35 (s). EI-MS: m/z exp. (calc.) 465.1453 found 466.1524 $[M + H]^+$.

4,5-Diphenyl-1,2-bis(3-(trifluoromethyl)phenyl)-1H-imidazole (m-CF_3PTPI-4). Yield: 80%, white solid, melting point = 205.3 °C, ^{1}H NMR (400 MHz, DMSO-d_6, TMS, δ ppm): 7.23−7.27 (1H, m), 7.31−7.34 (3H, m), 7.39−7.42 (1H, m), 7.45−7.49 (3H, m), 7.52−7.57 (5H, q), 7.73−7.74 (3H,d, J = 4 Hz), 8.38−8.40 (1H, m), 8.45 (1H, s). ^{13}C NMR (100 MHz, DMSO-d_6, TMS, δ ppm): 144.42 (s), 137.96 (s), 135.31 (s), 131.69 (s), 131.25 (s), 130.43 (s), 129.41 (s), 129.21 (dd, J = 7.5, 3.5 Hz), 128.91 (s), 128.73 (s), 127.58 (s), 127.58 (s), 127.20 (s), 126.32−125.92 (m), 125.04 (q, J = 3.9 Hz), 122.51−120.39 (m), 40.61 (s), 40.40 (s), 40.19 (s), 39.98 (s), 39.77 (s), 39.57 (s), 39.36 (s). EI-MS: m/z exp. (calc.) 508.1374 found 509.1437 $[M + H]^+$.

3-(4,5-Diphenyl-2-(3-(trifluoromethyl)phenyl)-1H-imidazol-1-yl)benzonitrile (m-CF_3PTPI-5). Yield: 80%, white solid, melting point = 210.5 °C, ^{1}H NMR (400 MHz, DMSO-d_6, TMS, δ ppm): 7.23−7.27 (2H, m), 7.31−7.34 (3H, m), 7.40−7.42 (2H, d, J = 4 Hz), 7.42−7.49 (2H, m), 7.52−7.57 (5H, q), 7.73−7.74 (3H, d, J = 8 Hz), 8.38−8.40 (1H, s). ^{13}C NMR (100 MHz, DMSO-d_6, TMS, δ ppm): 144.42 (s), 137.95 (s), 135.30 (s), 131.68 (s), 131.25 (s), 130.34 (d, J = 17.5 Hz), 129.55−129.09 (m), 128.82 (d, J = 18.4 Hz), 128.48 (s), 127.58 (s), 127.20 (s), 125.24 (dd, J = 7.5, 3.5 Hz), 121.88 (q, J = 3.1 Hz), 40.59 (s), 40.39 (s), 40.18 (s), 39.97 (s), 39.76 (s), 39.55 (s), 39.34 (s). EI-MS: m/z exp. (calc.) 465.1453 found 466.1510 $[M + H]^+$.

RESULTS AND DISCUSSION

Theoretical Calculations. It is highly relevant to understand the electronic structure of the designed luminophores, and prior to synthesizing, we have executed theoretical calculations. The structure of the luminophores was first optimized by DFT, and the excited-state electronic features were understood by TD-DFT. The ground-state optimized geometries and their FMO (frontier molecular orbitals) are shown in Figure 3, Figure S37, and Table ST3, and the corresponding values are given in Table 1. As shown in Figure S37 and Table ST3, the HOMO of electron clouds mainly dispersed on the diphenylimidazole moiety, which was expected to assist in hole transporting properties. On the other hand, the LUMO of m-CF_3PTPI-1, m-CF_3PTPI-2, and m-CF_3PTPI-4 were mainly distributed on the imidazole moiety, whereas the LUMO of m-CF_3PTPI-3 and m-CF_3PTPI-5 were mainly distributed on the cyano phenyl moiety. The electronic distribution patterns reveal their poor intramolecular charge transfer (ICT) property, which will trigger the achievement of blue or deep-blue emissions with wide bandgap energy.[29] The diphenylimidazole-based luminophores were presently designed, in which the substitution of EDGs and EWGs in the N1-position affected both HOMO and LUMO energy levels.[14] The fluorinated substitution into the fluorophores shows a low bandgap, which has been regarded as one of the promising strategies for improving the electroluminescence properties of OLED devices. The substitution of EDG (p-CH3) in the N1-position stabilized the HOMO energy level, and the electron-accepting substituent destabilized the HOMO energy level. m-CF_3PTPI-4 and m-CF_3PTPI-5 show the stabilized LUMO energy level as compared to the phenyl substitution in the N1-position. The theoretical UV−vis spectra were also obtained by the TD-DFT method in both gas and solvent phases, as depicted in Figure 4a,b, respectively. The intense absorption bands are observed in the luminophores, which is due to the $n \rightarrow \pi*$ transitions of the imidazole.

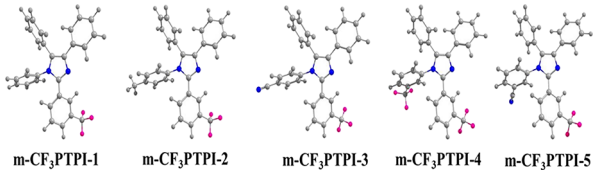

Figure 3. Ground-state optimized geometries of all the synthesized luminophores.

Charge Transport Properties. In determining the electrical properties of OLEDs, the balancing of charge injection and transfer characteristics of molecules is highly recommended, which decides the fate of efficient OLEDs. Thus, the energy barrier for injection and mobility of hole−electron must be determined by ionization potential (IP) and electron affinity (EA).[30−32,16] In general, lower IP and large EA values offer an obvious injection of holes and electrons. For all synthesized luminophores, λ represents the reorganization energy, which is calculated to evaluate the rate of charge transfer and balancing characteristics. For a potent charge transport process, a small λ value is required. In general, eqs 1 and 2 are used to determine the hole and electron transfers

$$\lambda_{hole} = [E^+(M) - E(M)] + [E^+(M^+) - E(M^+)]$$
$$\text{or } [\lambda_1 + \lambda_2] = IP_v - HEP \quad (1)$$

$$\lambda_{electron} = [E(M^-) - E^-(M^-)] + [E(M) - E^-(M)]$$
$$\text{or } [\lambda_3 + \lambda_4] = EEP - EA_v \quad (2)$$

The energies of the neutral, cation, and anion species are represented by E, E^+, and E^-, respectively, whereas M, M^+, and M^- stand for the optimized geometries of the neutral, cation, and anion, respectively. The hole and electron extraction potentials are represented by HEP and EEP, whereas HEP and EEP are the interpretations of IP and EA, respectively. The energy difference from M^+ to M gives HEP values using the M^+

Table 1. Theoretical Data of the m-CF_3PTPI Luminophores

luminophores	HOMO (eV)	LUMO (eV)	HOMO-1 (eV)	LUMO+1 (eV)	bandgap (eV)	singlet (eV)	triplet (eV)
m-CF_3PTPI-1	−5.65	−1.39	−6.72	−1.14	4.26	3.78	2.90
m-CF_3PTPI-2	−5.61	−1.35	−6.69	−1.09	4.26	3.79	2.90
m-CF_3PTPI-3	−5.91	−2.23	−6.91	−1.53	3.68	3.12	2.78
m-CF_3PTPI-4	−5.80	−1.70	−6.83	−1.61	4.10	3.52	2.87
m-CF_3PTPI-5	−5.88	−2.18	−6.88	−1.72	3.70	3.14	2.87

https://doi.org/10.1021/acs.jpcc.2c05220
J. Phys. Chem. C 2023, 127, 499−515

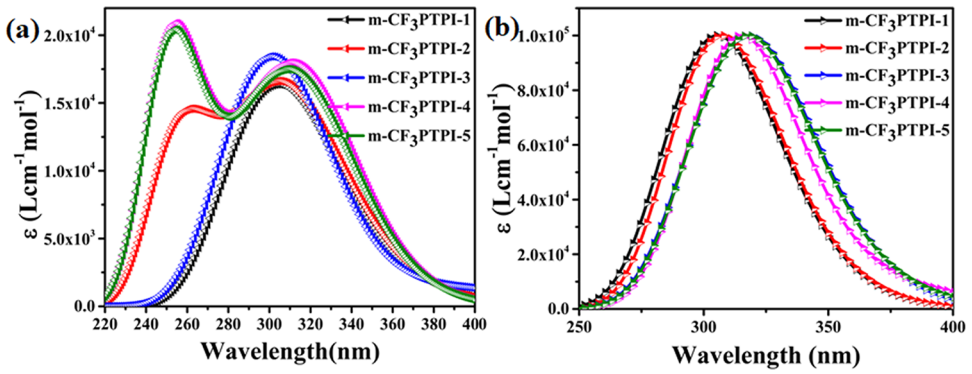

Figure 4. Theoretical UV−vis spectrum of m-CF_3PTPI luminophores in (a) the gas phase and (b) DCM obtained from DFT.

Table 2. Calculated Values of IP_v (eV), EAs (eV), Extraction Potentials (eV), and Reorganization Energies (eV) of Fluorophores

luminophores	m-CF_3PTPI-1	m-CF_3PTPI-2	m-CF_3PTPI-3	m-CF_3PTPI-4	m-CF_3PTPI-5	mcp
IP_v	7.061	7.011	7.310	7.186	7.255	6.80
HEP	6.695	6.648	6.927	6.799	6.890	
EEP	0.968	0.935	1.388	0.916	1.101	
$-EA_v$	0.337	0.313	0.998	0.679	0.945	0.15
λ_{hole}	0.365	0.362	0.382	0.386	0.365	0.06
$\lambda_{electron}$	0.631	0.621	0.390	0.237	0.155	0.12
$\Delta\lambda$	0.266	0.259	0.008	0.149	0.21	0.06

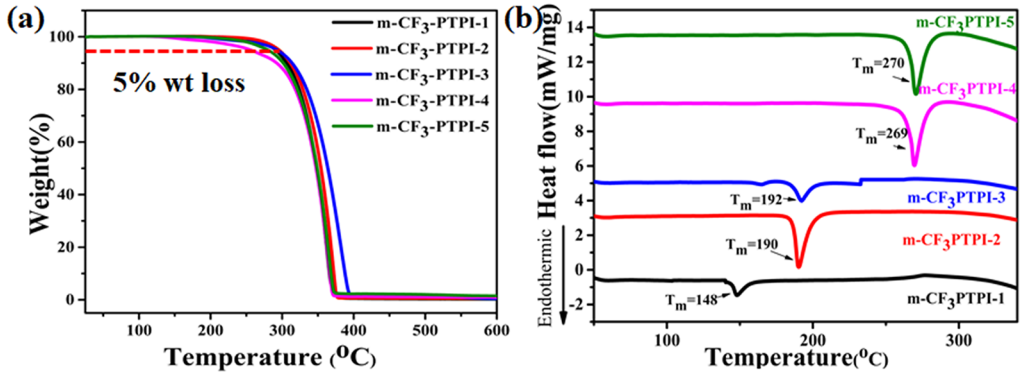

Figure 5. (a) TGA and (b) DSC curves of fluorophores at a heating rate of 10 °C/min in a nitrogen atmosphere.

geometric structure in the calculation, and the energy difference from M^- to M gives EEP using the M^- geometric structure in calculation. The energies of the neutral and cation species in their lowest energy geometry are represented by the $E(M)$ and $E^+(M^+)$, while the energies of the cation and neutral species are represented by $E(M^+)$ and $E^+(M)$, respectively. The estimated IP_v values in Table 2 rise in the following order: m-CF_3PTPI-2 < m-CF_3PTPI-1 < m-CF_3PTPI-4 < m-CF_3PTPI-5 < m-CF_3PTPI-3. The reorganization energies of electron transport ($\lambda_{electron}$) are somewhat greater than those of hole transport (λ_{hole}) for all luminophores, indicating that these luminophores' hole transport capacity is slightly better than their electron transport ability. Moreover, when the EWGs (CN and CF_3) are introduced on the core luminophores, the imbalances between λ_{hole} and $\lambda_{electron}$ for EWG-containing luminophores were smaller than those for the luminophores with EDGs, demonstrating that the performance of the OLED device is more affected for luminophores with EWGs. $\Delta\lambda$ for m-CF_3PTPI-3 is the lowest among all the fluorophores, which reveals that m-CF_3PTPI-3 has more potential as an emitter, which shows maximum brightness after blending with host materials. In addition, compared with all the luminophores, the luminophores with EWGs have more potential as emitters for OLED applications.

Thermal Properties. For highly efficient smart OLEDs, the prerequisite criterion is the morphological stability of the materials.[33] As shown by the TGA graph in Figure 5a, all these synthesized imidazole luminophores start to display weight loss (resultant 5% weight loss) at 258−296 °C, above the sublimation temperature (100 °C), revealing good thermal stability.[34] All the imidazole luminophores demonstrate almost similar decomposition enhancement except m-CF_3PTPI-4 because of their higher molecular mass.[35] However, similar decomposition enhancement is observed due to the structural framework.[36] The curves of heating DSC scans, which show the most exact T_m values of materials, are depicted in Figure 5b. It is seen that, although no distinct glass transition temperature (T_g) could be identified, the fluorophores show a good melting transition temperature from 148 to 270 °C. The superior thermal stability as well as endothermic melting

https://doi.org/10.1021/acs.jpcc.2c05220
J. Phys. Chem. C 2023, 127, 499−515

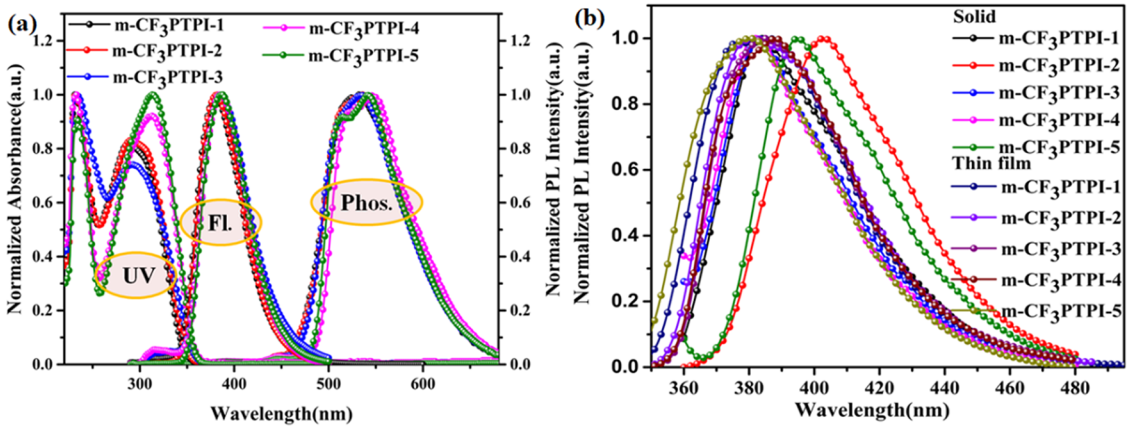

Figure 6. (a) UV−visible spectra, emission spectra at room temperature, and normalized phosphorescence spectra (77 K) of luminophores. (b) Emission spectra of the luminophores in solid and thin film.

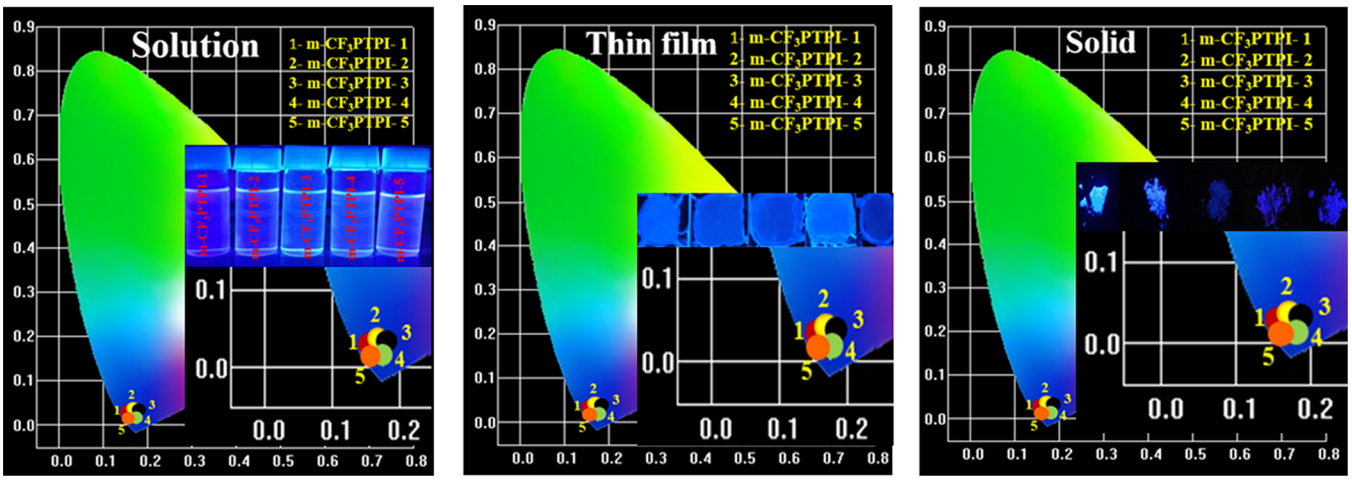

Figure 7. CIE coordinates of solution, thin film, and solid PL of the luminophores and images of the luminophores in solution, thin-film matrix, and solid under UV at 365 nm.

phenomena found in all the heating scans reveals the good morphological stability of amorphous films at high temperatures of the fluorophores, which is beneficial for lifetime operation as well as for device efficacy.[37,38] However, the materials are identified as well suited for OLED application.

Photophysical Properties. In common solvents like chloroform ($CHCl_3$), acetonitrile (ACN), methanol, tetrahydrofuran (THF), dichloromethane (DCM), dimethylformamide (DMF), dimethylsulfoxide (DMSO), and toluene, the luminophores are found to be soluble. The UV−visible spectra, emission spectra in DCM solution, and phosphorescence spectra are depicted in Figure 6, and their corresponding molar extinction coefficients have been calculated and are displayed in the Supporting Information (Figure S17). The luminophores show similar absorption wavelength at around 231 to 234 nm, which is due to the $\pi-\pi^*$ transitions of all the aromatic phenyl rings. The higher absorption wavelength at 289 to 314 nm is due to the $n-\pi^*$ transitions of the imidazole moieties containing an aromatic ring of the luminophores.[39−41] All the luminophores exhibited nearly related absorption spectra (shifting absorption maximum 8−20 nm) because of their comparable molecular frame as well as effective structural modification through EDGs and EWGs of different linkage positions.[42,43] The PL emission spectra of all the luminophores are recorded in DCM solution and depicted in Figure 6. It is observed that upon excitation at 280 nm, all luminophores display near UV/deep blue emission. m-CF_3PTPI-3, m-CF_3PTPI-4, and m-CF_3PTPI-5 showed deep blue emission in a higher PL emission band at around 395, 386, and 384 nm, respectively. m-CF_3PTPI-1 and m-CF_3PTPI-2 show an emission band in near UV at around 379 and 375 nm, respectively. The former are shown in a higher wavelength as compared to the latter because of the presence of electron-withdrawing moieties.[44]

The phosphorescence spectra suggest the location of the triplet energy level for the presently studied compounds; the emission was mainly found between 530 and 546 nm and be consigned of their phosphorescence from the triplet excited states. The triplet energies (E_T) were estimated from the highest-energy (0−0) vibronic sub-band of the phosphorescence spectra as 2.67 eV for m-CF_3PTPI-1, 2.63 eV for m-CF_3PTPI-2, 2.63 eV for m-CF_3PTPI-3, 2.54 eV for m-CF_3PTPI-4, and 2.58 eV for m-CF_3PTPI-5 (the trend is found to be similar to theoretically calculated triplet level energies). These phosphorescence spectra characteristics combined with E_T values indicate that they are sufficiently high enough to transfer energy from the host to dopant, and hence, they are capable of acting as hosts in green and red OLEDs;[42,45,46] based on this, we have used m-CF_3PTPI-1 and m-CF_3PTPI-2 as a host for green PhOLEDs.

https://doi.org/10.1021/acs.jpcc.2c05220
J. Phys. Chem. C 2023, 127, 499−515

Table 3. Photophysical and CIE Chromaticity Values of the Luminophores[a]

		λ_{em} (nm) (RT)			λ_{em} (nm) (77 K)		PLQY (Φ) (%)	CIE coordinates (x, y)		
luminophores	λ_{abs} (nm)	solution	PMMA film	solid	solution	E_T (eV)	solution	solution	PMMA film	solid
m-CF_3PTPI-1	232, 288	379	386	384	530	2.67	33.1	0.16, 0.01	0.15, 0.02	0.16, 0.01
m-CF_3PTPI-2	234, 295	375	382	402	535	2.63	30.0	0.15, 0.01	0.16, 0.01	0.16, 0.02
m-CF_3PTPI-3	233, 312	395	384	382	533	2.63	33.5	0.15, 0.01	0.15, 0.02	0.15, 0.02
m-CF_3PTPI-4	231, 309	386	388	381	519,546	2.54	20.3	0.16, 0.01	0.16, 0.01	0.15, 0.01
m-CF_3PTPI-5	234, 313	384	380	395	511,541	2.58	35.7	0.16, 0.01	0.16, 0.02	0.16, 0.01

[a]RT: room temperature, PLQY: photoluminescence quantum yield.

On the other hand, assessment with the solution, solid, and thin film emission spectra is also observed in the deep blue region. Figure 6b shows the solid and thin film emission spectra, which exhibit small shifting to a longer wavelength compared to the solution emission spectra around 382−402 and 378−390 nm, respectively. Therefore, the obtained results showed that all the luminophores emit in the deep blue region and the CIE_y color coordinates are <0.1, which satisfy the NTSC standard.[47] The digital images of all the luminophores in solid, solution (DCM), and thin films are taken under a 365 nm UV lamp and are given in Figure 7. The corresponding data of the photophysical study and photoluminescence quantum yield (PLQY) are measured in DCM solution, and the obtained values are summarized in Table 3.

Electrochemical Analysis. The electrochemical properties of the luminophores were studied by cyclic voltammetry (CV) in DMF solvent with 0.1 M tetrabutylammonium hexafluorophosphate ($TBAPF_6$) as a supporting electrolyte using a three-standard electrode under a N_2 atmosphere. Imidazole luminophores showed onset oxidation potentials and onset reduction potentials at 1.32 to 1.19 V and −1.12 to −1.75 V ranges. The HOMO and LUMO energy levels of imidazole luminophores were determined from the onset oxidation potentials and onset reduction potentials, and the energy levels were estimated by using Leeuw *et al.*'s equations (eqs 3 and 4)[46]

$$E_{HOMO} = -(E_{ox}^{onset} + 4.4)eV \quad (3)$$

$$E_{LUMO} = -(E_{red}^{onset} + 4.4)eV \quad (4)$$

The corresponding oxidation and reduction potentials and their HOMO and LUMO energy levels are given in Table 4. It

Table 4. Key Data of Electrochemical Analysis of the Luminophores under a N_2 Atmosphere

luminophores	E_{ox}^{onset} (V)	E_{red}^{onset} (V)	HOMO (eV)	LUMO (eV)	bandgap (eV)
m-CF_3PTPI-1	1.32	−1.51	−5.72	−2.88	2.83
m-CF_3PTPI-2	1.49	−1.75	−5.89	−2.64	3.24
m-CF_3PTPI-3	1.19	−1.12	−5.59	−3.27	2.32
m-CF_3PTPI-4	1.19	−1.19	−5.59	−3.20	2.39
m-CF_3PTPI-5	1.21	−1.14	−5.61	−3.25	2.36

is observed that deep HOMO and LUMO energy levels possess good electron and hole transportation properties.[48] The decrease in oxidation potential follows the corresponding order of inductive effect of the substituents: CH_3 > H > CF_3, which is due to the presence of the inductive effect caused by the different substituents (−ve effect for fluorine and +ve effect for the methyl group).[49] The comparison of the HOMO−LUMO energy gap of all the fluorophores indicates that the HOMO/LUMO energy levels change with respect to that of the N_1 substitution of imidazole. However, the larger bandgap further proves the powerful structural adjustment for controllable emissions by simply changing the linkage modes.[50] Among all, m-CF_3PTPI-3, m-CF_3PTPI-4, and m-CF_3PTPI-5 with EWGs present result in lowering the bandgap, in agreement with the PL data. As we know from DFT, the energy gap is less for EWGs as compared to EDGs, whereas electrochemical analysis also follows the same trend as theoretical calculations. Accordingly, the electrochemical diagram and their corresponding data of the imidazole derivatives are summarized in Figure 8 and Table 4.

Electroluminescence. To further explore the viable applications of diphenylimidazole derivative-based luminophores, OLEDs encouraged us to study them experimentally. The EL performance of the synthesized diphenylimidazole derivative-based materials was employed both as an emitter and host, studying a series of OLED devices designed and fabricated via the solution process. The device structures were fabricated with multilayer configuration using blue emitter luminophores, as shown in the schematic diagram of the device (Figure 9a) and their corresponding energy level diagrams (Figure 9b). The luminophores were used as emitters at different concentrations (1.0, 3.0, and 5.0 wt %) with CBP as a host. The device configuration was ITO (125 nm)/PEDOT:PSS (35 nm)/CBP:1, 3, and 5 wt % m-CF_3PTPI-1, m-CF_3PTPI-2, m-CF_3PTPI-3, m-CF_3PTPI-4, or m-CF_3PTPI-5 (20 nm)/TPBi (40 nm)/LiF (1 nm)/Al (200 nm).

The current density−voltage−luminescence (J-V-L) characteristics and EL spectra of the fabricated doped OLED devices are displayed in Figure 10 and Figures S38−S41, and their corresponding EL properties are summarized in Table 5. The m-CF_3PTPI-1 emitter-based device shows bluish-white emission at a CIE coordinate of (0.28, 0.34). The doped OLED devices were structured to enhance the color purity and device efficiency of the synthesized emitters. Here, CBP is utilized as a host material due to its suitable HOMO and LUMO level with the emitter and the bipolar property to ensure efficient charge transfer to the emitters. Doping concentrations ranged from 1.0 to 5.0 wt %, and the device displayed high brightness, low current density, and improved efficiency. It is noted that, compared with the undoped device, the doped device showed the best device performance. Better EL properties may be related to the (a) effective host−dopant energy transfer, (b) suitable matching of HOMO−LUMO and triplet energy of the host with the dopant's, (c) balanced charge carriers (holes and electrons) in the recombination region, and (d) feasibility of radiative exciton formation.[17,51,52]

From the EL spectra and tabulated EL properties, it is clear that the devices show near-UV emission at CIE coordinates (0.16, 0.09) to (0.17, 0.11) with EL peaks in the range of 380−395 nm. The displayed CIE coordinates are in very close

https://doi.org/10.1021/acs.jpcc.2c05220
J. Phys. Chem. C 2023, 127, 499−515

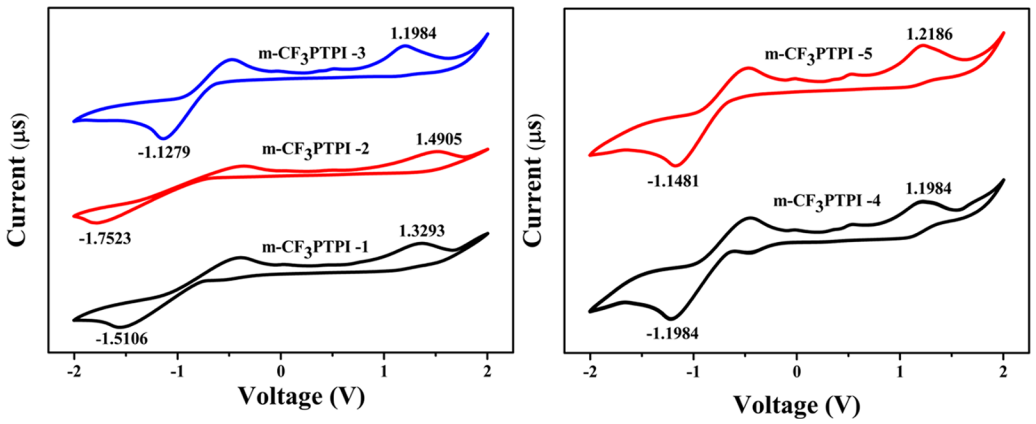

Figure 8. CV of the luminophores in DMF under a N_2 atmosphere.

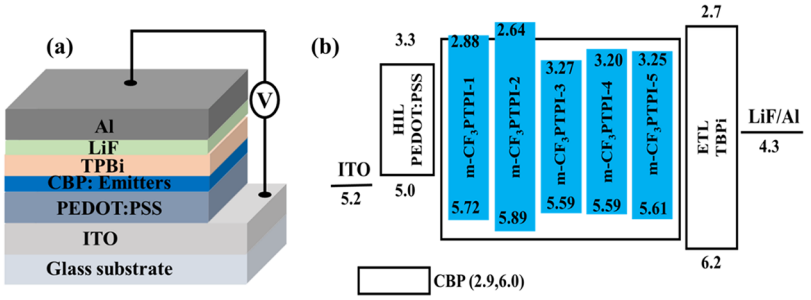

Figure 9. (a) Schematic device structure and (b) energy level diagram of OLED devices incorporated with diphenylimidazole derivative-based blue emitter m-CF_3PTPI-1, m-CF_3PTPI-2, m-CF_3PTPI-3, m-CF_3PTPI-4, or m-CF_3PTPI-5 with CBP as the host.

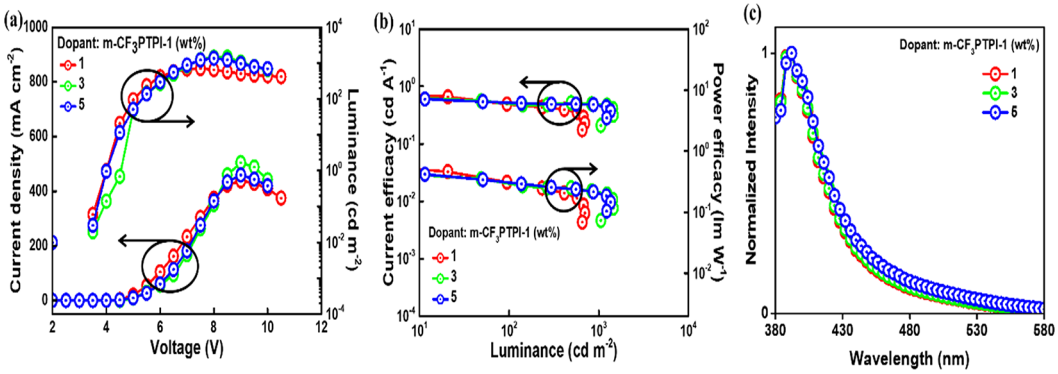

Figure 10. (a) Luminance−voltage−current density (L-V-J), (b) power efficacy−luminance−current efficacy, and (c) electroluminescence spectra of blue OLED incorporated with diphenylimidazole derivative-based emitter m-CF_3PTPI-1 at concentrations 1.0, 3.0, and 5.0 wt % in the CBP host matrix.

proximity to the NTSC determined standard blue coordinates (0.14, 0.08). The peaks of the EL spectra (~395 nm) of the devices are more similar to the observed PL of the emitters in the thin film and DCM solution, indicative of the origin of the emission in the EL and symbolizing the radiative decay of a singlet exciton localized on the guest without any aggregates between the thin film and molecules.

Furthermore, the CIE coordinates for the doped sample displayed purer blue color than nondoped ones. The reason behind may be attributed to the difference in the polarity of the host and dopant in the solid film. Moreover, it is noteworthy that on increasing the concentration of the doped devices, negligible change is observed in the spectra peak with a minor to no red shift in some devices, confirming the stability even at higher concentrations. To analyze, the best performing device, m-CF_3PTPI-5 (3.0 wt %), displayed a PE of 0.9 lm/W, CE of 1.3 cd/A, and EQE of 2.8% at a brightness of 953 cd/m^2. The reason behind may be the matching of energy levels for the host and dopant, which favors balanced charge transport, and effective host to dopant energy transfer.

To improve the performance further, Figure 11 shows the overlapping area between the absorbance of the emitter and PL of various hosts. The importance of this observation is that the higher the overlapping area between the absorbance and PL spectra, the better will be the charge transporting capability between them and the better will be the performance. Three hosts, namely, SimCP2, mCP, and Spiro-2-CBP, were chosen due to their wider bandgap, higher triplet energy, and larger overlapping as compared to those of the counterpart CBP host. Therefore, SimCP2 was the most overlapping among all and

https://doi.org/10.1021/acs.jpcc.2c05220
J. Phys. Chem. C 2023, 127, 499−515

Table 5. Electroluminescence Properties of Emitters (Doped/Undoped) in the CBP Host Matrix at Varying Concentrations

dopant	doping con. (wt %)	turn-on voltage (V)	$PE_{100}/CE_{100}/EQE_{100}$ (lm/W/cd/A/%)	$PE_{1000}/CE_{1000}/EQE_{1000}$ (lm/W/cd/A/%)	$PE_{max}/CE_{max}/EQE_{max}$ (lm/W/cd/A/%)	CIExy coordinates	Maxi. Lum. (cd/m^2)
m-CF_3PTPI-1	1	4.2	0.3/0.5/1.5	-/-/-	0.6/0.8/2.0	(0.16, 0.09)/-	700
	3	4.1	0.4/0.7/1.9	0.19/0.42/0.53	0.53/0.76/2.0	(0.16, 0.10)/(0.16, 0.10)	1046
	5	5.0	0.2/0.5/1.2	0.1/0.3/0.3	0.5/0.7/1.22	(0.17, 0.11)/(0.19, 0.18)	1399
m-CF_3PTPI-2	1	5.1	0.3/0.5/1.4	-/-/-	0.5/0.7/1.9	(0.17, 0.10)/-	635
	3	4.2	0.3/0.5/1.6	0.2/0.5/0.7	0.6/0.8/1.9	(0.16, 0.09)/(0.18, 0.15)	1290
	5	3.7	0.4/0.6/1.6	0.1/0.3/0.3	0.7/0.9/1.7	(0.16, 0.10)/(0.20, 0.20)	1340
m-CF_3PTPI-3	1	4.6	0.3/0.5/1.5	0.07/0.1/0.1	0.3/0.5/1.5	(0.16, 0.09)/(0.22, 0.23)	1020
	3	4.1	0.3/0.6/1.6	0.3/0.6/1.0	0.6/0.8/1.9	(0.16, 0.09)/(0.18, 0.13)	1175
	5	4.9	0.3/0.6/1.5	0.2/0.5/0.7	0.5/0.7/1.7	(0.16, 0.09)/(0.18, 0.15)	1731
m-CF_3PTPI-4	1	4.7	03/0.5/1.8	0.1/0.2/0.1	0.3/0.6/2.2	(0.16, 0.09)/(0.21, 0.21)	1146
	3	4.3	0.3/0.5/1.6	0.2/0.5/0.5	0.3/0.5/1.6	(0.16, 0.09)/(0.19, 0.16)	1029
	5	5.3	0.1/0.3/0.1	-/-/-	0.1/0.3/0.1	(0.16, 0.09)	930
m-CF_3PTPI-5	1	4.1	0.3/0.6/1.7	-/-/-	0.5/0.8/2.7	(0.17, 0.10)	753
	3	4.1	0.3/0.6/1.6	-/-/-	0.9/1.3/2.8	(0.17, 0.10)	953
	5	3.7	0.5/0.7/1.7	0.2/0.5/0.5	0.9/1.2/2.6	(0.17, 0.10)/(0.19, 0.15)	1321

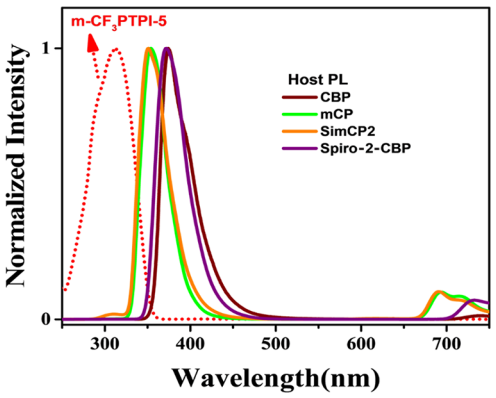

Figure 11. Overlapping between an absorption spectrum of emitter m-CF_3PTPI-5 and PL spectra of different hosts.

showed the best performance with a maximum EQE of 4.0% that is very close to the theoretical limit of fluorescent emitters, as shown in Figure 11. The best performing emitter m-CF_3PTPI-5 was selected to carry out further analysis.

Figure 12 shows the energy-level diagram of a blue OLED using different hosts doped with a 3 wt % m-CF_3PTPI-5

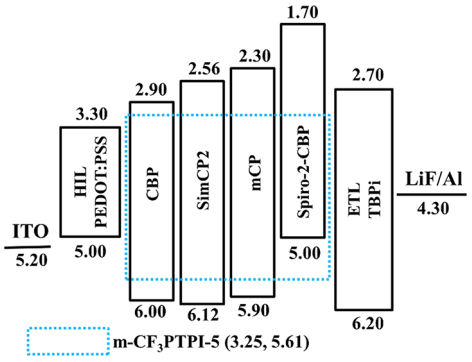

Figure 12. Energy-level diagram of the blue OLED composed of an emitter m-CF_3PTPI-5 in different host matrixes.

emitter. Three other hosts, namely, SimCP2, mCP, and Spiro-2-CBP, were utilized. Among all, SimCP2 possesses an extremely large bandgap of 3.56 eV and shows a maximum overlapping with the emitter. Table ST4 shows the comparison of PE, CE, EQE, turn-on voltage, CIE, and luminance of devices based on different hosts doped with a 3 wt % m-CF_3PTPI-5 emitter.

Figure 13a,b shows the J-V-L and efficacy performance of the devices. SimCP2-based devices displayed a high current density and an L_{max} of 2980 cd/m^2. The device also showed a low turn-on voltage of 3.9 V and EQE_{max} of 4.0% that is close to the theoretical limit of fluorescent materials (Table ST4). An absence of an additional peak in the EL spectra (as shown in Figure 13c) is indicative of the complete transfer of energy from the host to guest. However, a slight red shift is observed in the SimCP2-based device compared to the CBP-based one, which may be attributed to an electron barrier of 0.14 eV, which might have hindered the smooth transportation of electrons into the emissive layer.

Figure 14 depicts the (panel a) schematic device structure and (panel b) the energy level diagram for the wet-processed OLEDs using hosts m-CF_3PTPI-1 and m-CF_3PTPI-2 doped with a green phosphorescent dye $Ir(ppy)_3$. It is interesting to

https://doi.org/10.1021/acs.jpcc.2c05220
J. Phys. Chem. C 2023, 127, 499−515

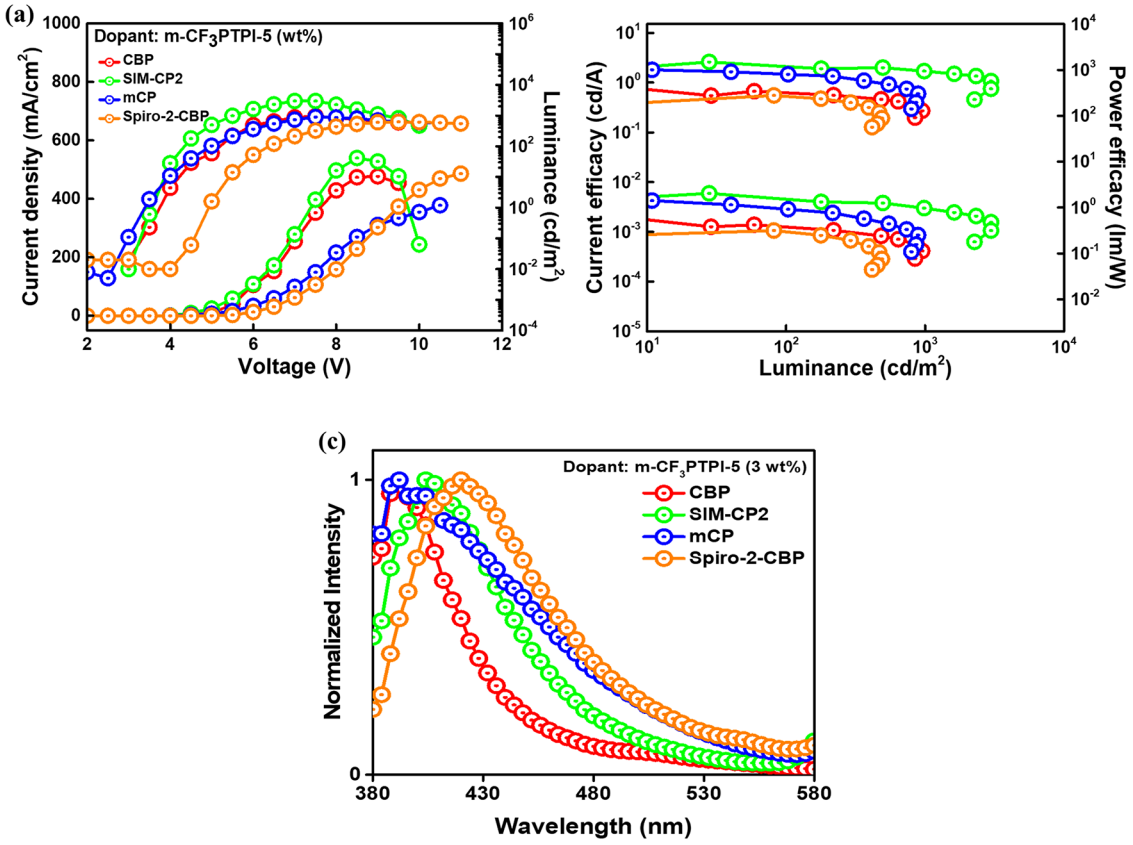

Figure 13. (a) Current density−voltage−luminance, (b) current efficiency−luminance−power efficiency plots, and (c) EL spectra of the blue OLED composed of the m-CF_3PTPI-5 emitter doped in different host matrixes.

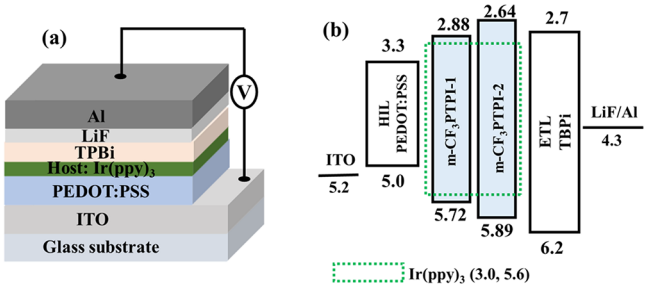

Figure 14. (a) Schematic device structure and (b) energy level diagram of materials m-CF_3PTPI-1 and m-CF_3PTPI-2 used as hosts with a green phosphorescent dopant $Ir(ppy)_3$.

note that the materials m-CF_3PTPI-1 and m-CF_3PTPI-2 are bifunctional materials working both as an emitter and host. Moreover, the performance of these materials was sharply increased when used as a host, which is credited to the large HOMO−LUMO gap (>2.8 eV) suitable to transfer energy to the guest singlet energy level. Thereby, the device was structured as ITO (125 nm)/PEDOT:PSS (35 nm)/m-CF_3PTPI-1 or m-CF_3PTPI-2:7.5, 10, 12.5, and 15 wt % $Ir(ppy)_3$ (20 nm)/TPBi (40 nm)/LiF (1 nm)/Al (200 nm). The dopant $Ir(ppy)_3$ is chosen due to its large HOMO−LUMO levels suitable with the host materials, and the concentrations were precisely optimized for a greater host−guest energy transfer.

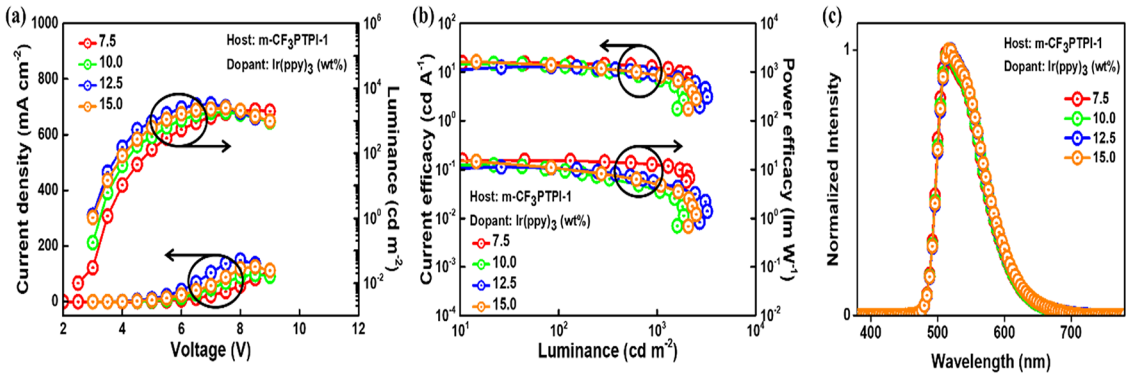

Figure 15. Electroluminescence properties of host m-CF_3PTPI-1 with green phosphorescent dye at concentrations 7.5, 10.0, 12.5, and 15.0 wt % showing (a) current density−voltage−luminance (J-V-L), (b) current efficacy−luminance−power efficacy, and (c) electroluminescence spectra.

https://doi.org/10.1021/acs.jpcc.2c05220
J. Phys. Chem. C 2023, 127, 499−515

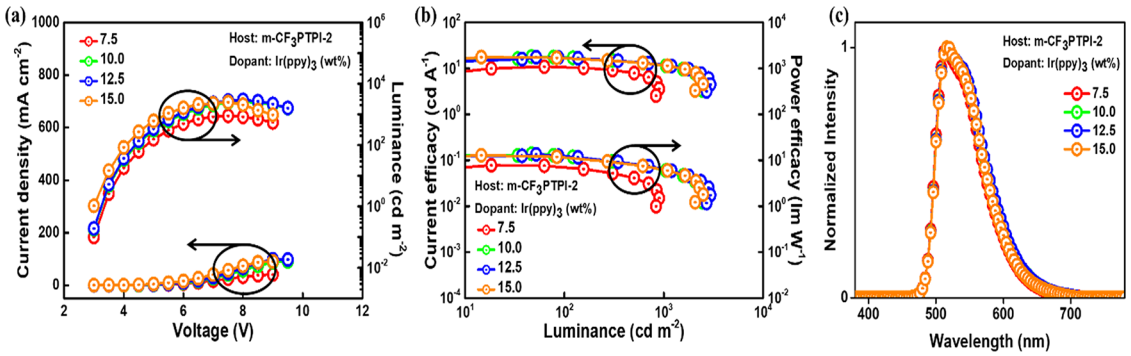

Figure 16. Electroluminescence properties of host m-CF_3PTPI-2 with green phosphorescent dye at concentrations 7.5, 10.0, 12.5, and 15.0 wt % showing (a) current density−voltage−luminance (J-V-L), (b) current efficacy−luminance−power efficacy, and (c) electroluminescence spectra.

Table 6. Electroluminescence Properties of Hosts m-CF_3PTPI-1 and m-CF_3PTPI-2 Doped in Green Phosphorescent Dye Ir(ppy)$_3$ at Varying Concentrations

host	dopant	doping con. (wt %)	turn-on voltage (V)	$PE_{100}/CE_{100}/EQE_{100}$ (lm/W/cd/A/%)	$PE_{1000}/CE_{1000}/EQE_{1000}$ (lm/W/cd/A/%)	$PE_{max}/CE_{max}/EQE_{max}$ (lm/W/cd/A/%)	CIExy coordinates	Maxi. Lum. (cd/m^2)
m-CF_3PTPI-1	Ir(ppy)$_3$	7.5	4.0	5.6/9.8/2.7	2.6/5.8/0.8	12.0/15.3/4.2	(0.30, 0.62)/ (0.30, 0.62)	2125
		10	3.9	10.5/14.0/3.4	3.6/6.8/1.9	12.4/15.0/4.1	(0.31, 0.62)/ (0.30, 0.62)	1864
		12.5	3.3	10.7/13.0/3.5	5.5/8.9/2.4	10.7/13.0/3.5	(0.31, 0.62)/ (0.31, 0.62)	3229
		15	3.4	10.9/13.9/3.8	4.7/8.3/2.3	16.4/15.7/4.3	(0.31, 0.62)/ (0.31, 0.62)	3688
m-CF_3PTPI-2		7.5	3.7	7.5/10.8/3.0	-/-/-	7.7/10.8/3.0	(0.31, 0.62)/ (0.31, 0.62)	901
		10	3.9	11.8/16.9/4.7	5.9/11.4/3.1	13.7/17.9/4.9	(0.32, 0.61)/ (0.32, 0.61)	1948
		12.5	3.6	12.5/17.1/4.7	5.8/11.2/3.1	13.4/17.5/4.8	(0.32, 0.61)/ (0.32, 0.61)	4695
		15	3.6	11.6/16.5/4.6	4.5/9.4/2.6	12.5/17.1/4.7	(0.32, 0.61)/ (0.32, 0.61)	2505

On fabricating the devices using m-CF_3PTPI-1 and m-CF_3PTPI-2 as a host, the current density−voltage−luminance (J-V-L) characteristics were sharply improved with significant increments, as seen in Figures 15 and 16. The electroluminescence spectra are red shifted due to the presence of green dye, and a peak at around 525 nm was observed. The CIE coordinates (0.31, 0.62) thus observed lie in the yellowish-green region of chromaticity spectrum. The shifting may be attributed to the radiative emission from the dopant's singlet state.

Further, a clear understanding has been drawn from Table 6, which summarizes the EL properties of both the host doped with 7.5, 10.0, 12.5, and 15.0 wt % doping concentrations in the green dye. m-CF_3PTPI-2, due to its good hole-blocking ability, achieves an EQE_{max} of 4.9%, CE_{max} of 17.9 cd/A, and PE_{max} of 13.7 lm/W at a 10 wt % doping concentration. The 1948 cd/m^2 L_{max} for the same device is comparatively less and may be attributed to insufficient charge balance due to a higher LUMO level than the ETL (TPBi).

Chemosensing. The sensing behaviors of imidazole-based luminophores were thoroughly analyzed by fluorescence spectroscopy. The imidazole-based molecules show strong fluorescence, which can be the most interesting successor for chemosensors. The detection of fluorescence quenching reveals the rather low LUMO energies of PH, BA, and the nitro-containing explosive compounds such as 4-NP, 2,4-DNP, and PA, which may withdraw electrons from the excited-state fluorophores via a photo-induced electron transfer (PET) quenching process.[53] m-CF_3PTPI luminophores were dissolved in THF solution (1×10^{-5} M), and their sensing properties were studied. Then, further different nitroaromatic compounds were subsequently added into the solution to examine the difference in the fluorescence intensity of the luminophores. Figure 17 shows that the luminophores' fluorescence intensity steadily decreased by adding different quenchers. Among all the nitro explosive quenchers, the fast reaction can be ascribed to PA, which displayed a higher fluorescence quenching over other nitro explosives, due to the lower value of the LUMO energy level of PA, as shown in Figure 18. As compared with other nitro explosives, the fluorescence intensity gradually decreases with increasing PA concentration. To confirm the mechanism of interaction among the nitrogen's lone pair and hydroxyl group of quenchers, we performed quenching experiments by taking 2,4-dinitrotoluene (DNT) instead of hydroxyl quenchers, as shown in Figure S26 (Supporting Information). The results reveal that by gradual addition of DNT (0 to 300 μM), very negligible change in intensity can be seen, which suggests that the methyl group in DNT does not interact with nitrogen's lone pair of our designed fluorophores. The quenching efficiency plots of all the luminophores with the quenchers are shown in Figure S36. Among all the fluorophores, m-CF_3PTPI-2 shows a maximum quenching efficiency of 87% because of its electron-donating group, which enhances the

https://doi.org/10.1021/acs.jpcc.2c05220
J. Phys. Chem. C 2023, 127, 499−515

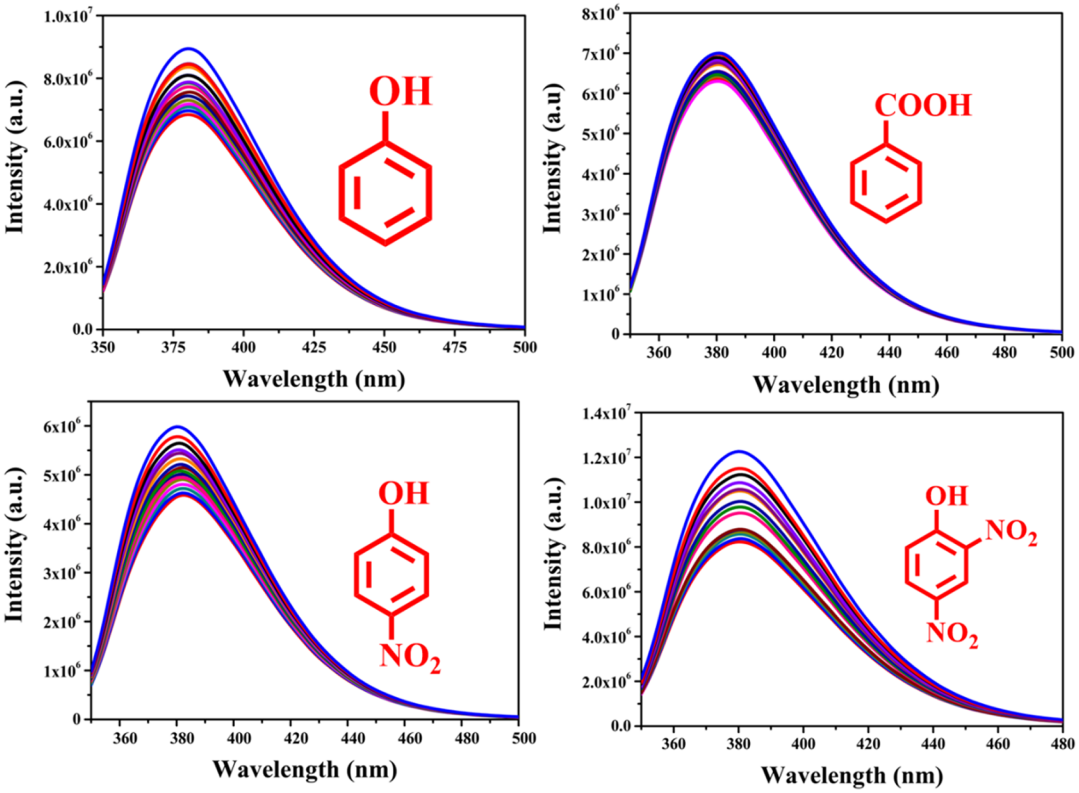

Figure 17. Difference in the fluorescence intensity of m-CF_3PTPI-1 after addition of different quenchers.

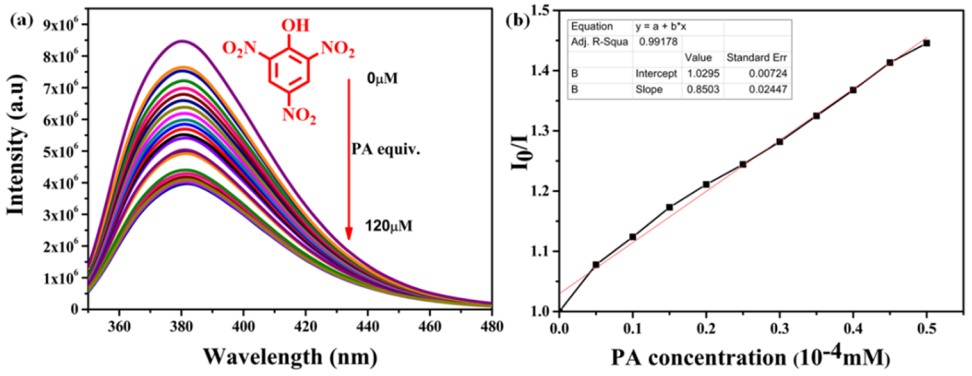

Figure 18. Difference in the fluorescence intensity of m-CF_3PTPI-1 after addition of PA. (b) K_{SV} of m-CF_3PTPI-1 using PA as a quencher.

interaction with the electron-deficient PA. It clearly shows that luminophores with PA show maximum quenching efficiency in comparison with other quenchers. The quenching constant was calculated by using Stern−Volmer (K_{SV}) equation[54]

$$I_0/I = 1 + K_{SV}[Q]$$

where the PL intensities before and after the addition of PA are represented by I_0 and I, the quencher concentration is defined by $[Q]$, and the Stern−Volmer quenching constant is represented by K_{SV}. The fluorescence and the K_{SV} plots (I_0/I vs PA concentration) of m-CF_3PTPI-1 are presented in Figure 18, and the other four luminophores are presented in Figures S18−S25. The K_{SV} values of all the luminophores were found in the range of 0.25×10^4 to 1.55×10^4 M^{-1}, which is comparable with the reported values shown in Table ST2.

As indicated in the K_{SV} plots, bending upward curves are owed to the super amplified quenching effect, revealing that upon addition of PA concentration, the quenching of luminescence becomes more efficient.[22] The fluorescence spectra of the remaining luminophores (m-CF_3PTPI-2 to m-CF_3PTPI-5) with PA and K_{SV} plots are shown in Supporting Information (Figures S18−S25). When the concentration of PA was relatively low, then the K_{SV} curve was found to be linear with a correlation coefficient (R^2) of 0.995 and resulting quenching constant of 0.85×10^4, demonstrating the static quenching interaction between the luminophores and PA. Fascinatingly, the quenching efficiency of m-CF_3PTPI-2 toward PA is found to be 87% higher than other luminophores (Figure S36). Due to the strong acidic behavior of PA, it can easily transfer an acidic proton to the basic functional group of the luminophores. The presence of EDGs in N1 positions enhances the basicity of the imidazole ring, resulting in the strong interaction with acidic PA, which leads to the fluorescence quenching of the luminophores.[24]

Further, the digital photographs of Figure 19 clearly show that the color of luminophores changed from blue to colorless

https://doi.org/10.1021/acs.jpcc.2c05220
J. Phys. Chem. C 2023, 127, 499−515

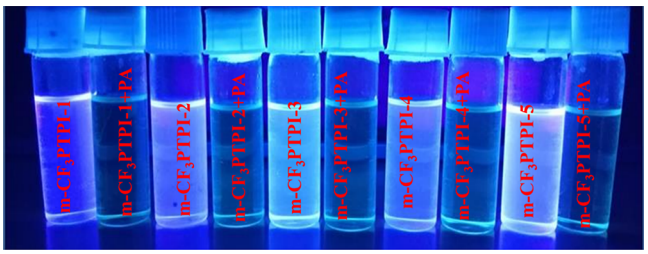

Figure 19. Digital images of luminophores in the solution phase under a UV lamp before and after addition of PA.

in the presence of PA. Also, in the theoretical study that we have done, the LUMO energy level of PA is in between all the luminophores of HOMO and LUMO energy level. This concludes that the PET is the foremost cause for fluorescence quenching of the luminophores.

As shown in Figure 20, ^{1}H NMR spectroscopy was utilized to clarify the interaction between the m-CF_3PTPI-1 luminophores and PA in solution. The shifting signal associated with the PA proton confirms that there is formation of a complex with imidazole nitrogen and PA. With the gradual increase in PA concentration, the signal moves further up field, suggesting a strong electrostatic interaction between PA and luminophores.[53] The NMR spectra of other imidazole-based luminophores with PA showed a similar behavior, and the spectra are displayed in the Supporting Information Figures S27−S30.

In the mechanistic quenching of the luminophores (m-CF_3PTPI-1 to m-CF_3PTPI-5), the lifetime of the luminophores was determined in the presence and absence of PA, and their results are shown in the Supporting Information (Figure S35 and Table ST1). It is interesting to note that after adding the quencher (PA) to the luminophores, a decrease in lifetime has been observed by few nanoseconds, which clearly indicates that PA acts as a quencher.

Mechanism for the PA Detection Limit. The PA detection limit (DL) can be obtained by calibrating the fluorescence intensity of m-CF_3PTPI-1 to m-CF_3PTPI-5 in THF solvent with PA solution (10^{-6} M). The analogous fluorescence intensity as a function of gradual addition of PA is shown in Figure 21. The DL of PA can be calculated by using the following equation (eq 5)[55]

$$\mathrm{DL} = C_L \times C_T \tag{5}$$

The concentrations of luminophores and the concentrations of PA at which a steep decrease is observed are defined by C_L and C_T, respectively. DL values are found in the range of 104−249 ppb, and the values are given in Table 7 and Table ST2. The currently observed DL values were compared with the reported similar small molecular fluorescent PA sensors and found to indicate better sensitivity (for more examples, Table ST2 in the SI).[16,56] Among all, the highest sensitivity was observed for m-CF_3PTPI-2 toward PA, which is due to more electron-donating methyl group, which offers easy interaction with PA.[57]

Mechanism for PA Detection by DFT Analysis. Furthermore, to know the origin of PA sensitivity, the FMO of PA and m-CF_3PTPI derivatives (m-CF_3PTPI-1 to m-CF_3PTPI-5) were determined by DFT. The LUMO and HOMO energy levels of PA are −4.52 and −8.58 eV, respectively. This value is in between the calculated energy levels of m-CF_3PTPI-1 to m-CF_3PTPI-5. Figure 22a shows that the PET process is the major contribution to the fluorescence quenching of luminophores by the addition of PA. Additionally, after the interaction of PA to luminophores, the internal charge transfer (ICT) process was confirmed through FMO study. Here, in all the cases, the electron cloud particularly localized on the phenyl groups of luminophores in the case of HOMO and LUMO dispersed over the imidazole group of luminophores. After the interaction of PA with luminophores, the orbital distribution pattern was changed, as shown in Figure 22b. Thus, after binding of PA

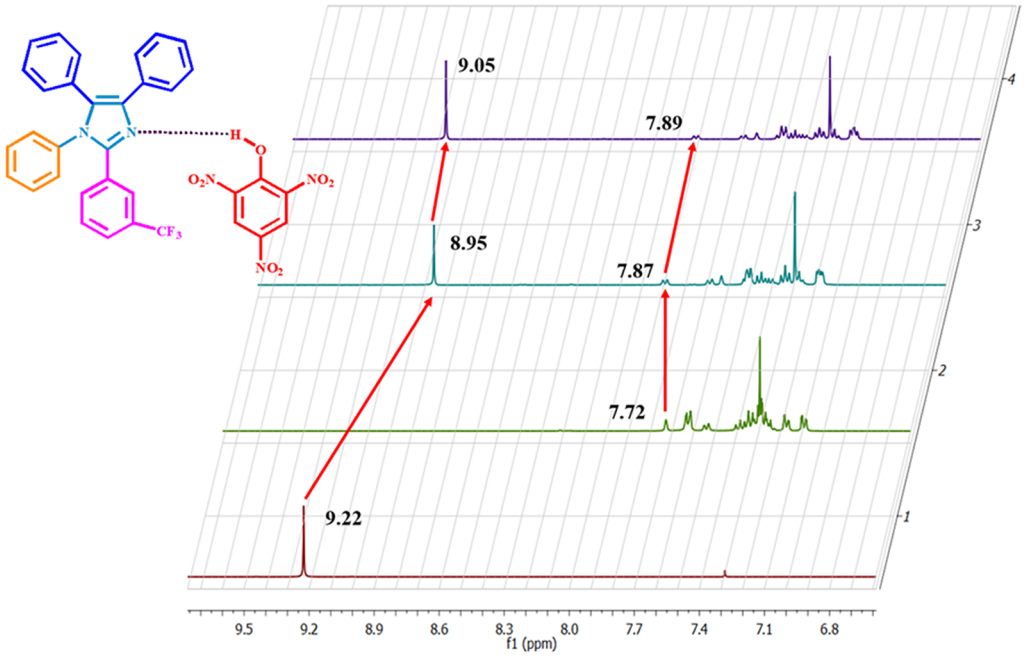

Figure 20. ^{1}H NMR spectrum of m-CF_3PTPI-1 with PA (0, 0.5, and 1.0 equiv) in $CDCl_3$.

https://doi.org/10.1021/acs.jpcc.2c05220
J. Phys. Chem. C 2023, 127, 499−515

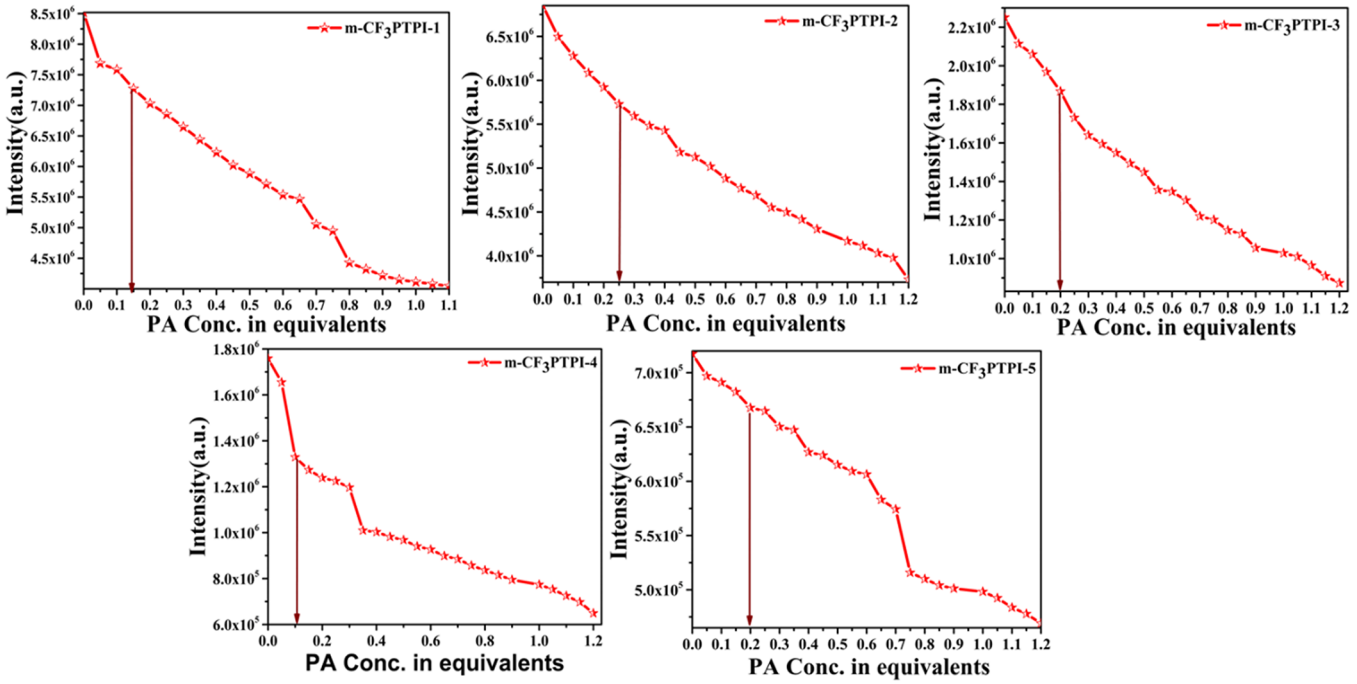

Figure 21. Fluorescence intensity of m-CF_3PTPI luminophores as a function of PA concentration.

Table 7. Luminophores and Their Stern−Volmer Constants and Detection Limits

luminophores	Stern−Volmer constant (K_{SV}) ($10^4 \times M^{-1}$)	detection limit (ppb)
m-CF_3PTPI-1	0.85	148
m-CF_3PTPI-2	0.67	249
m-CF_3PTPI-3	1.18	199
m-CF_3PTPI-4	1.55	104
m-CF_3PTPI-5	0.25	194

with luminophores, which results in the decrease in energy clearly, the formation of a stronger charge transfer complex of luminophores with PA is pointed out.[24] The FMO orbitals of the remaining luminophores (m-CF_3PTPI-2 to m-CF_3PTPI-5) with PA are shown in the Supporting Information (Figures S31−S34).

CONCLUSIONS

In this work, we have successfully synthesized the unipolar compounds m-CF_3PTPI-1, m-CF_3PTPI-2, m-CF_3PTPI-3, m-CF_3PTPI-4, and m-CF_3PTPI-5 and fabricated near UV/deep blue OLED devices. All the fluorophores showed near UV/deep blue emission with excellent CIE values. In addition, the triplet energy of the luminophores was found be >2.5 eV. Among all the doped devices, the 3.0 wt % doped m-CF_3PTPI-5 in the CBP host matrix showed a better performance with a PE_{max} of 0.9 lm W^{-1}, CE_{max} of 1.3 cd A^{-1}, and EQE_{max} of 2.82%. Later, due to wide HOMO−LUMO level range/high triplet energy, we have utilized two compounds m-CF_3PTPI-1 and m-CF_3PTPI-2 as a host doped with a green phosphorescent dopant $Ir(ppy)_3$ at varying concentrations and depicted that the 10 wt % doped m-CF_3PTPI-2 OLED device performs better with an EQE_{max} of 4.9% and CE_{max} of 17.9 cd A^{-1}. This device showed a slight red shift with the emission peaked at 525 nm, emitting yellowish-green light. Therefore, the materials possess a bifunctional property and the optimized

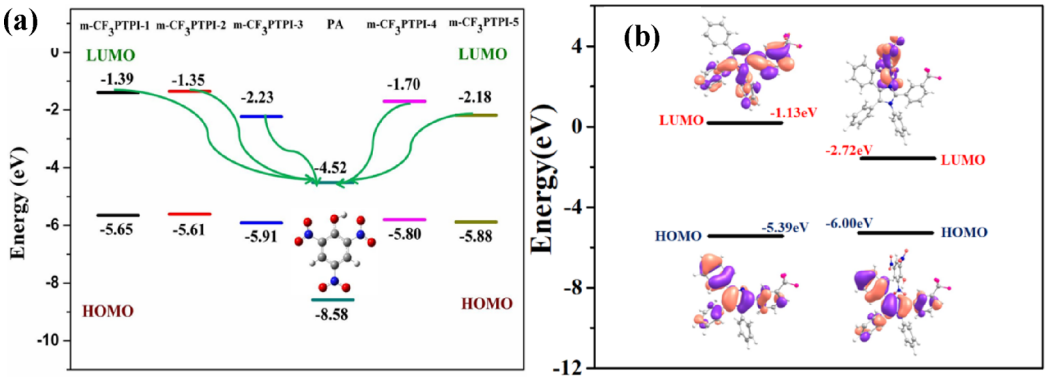

Figure 22. (a) Electron transfer process between luminophores (m-CF_3PTPI-1 to m-CF_3PTPI-5) and PA and (b) FMO of m-CF_3PTPI-1 and m-CF_3PTPI-1 + PA obtained from the DFT.

https://doi.org/10.1021/acs.jpcc.2c05220
J. Phys. Chem. C 2023, 127, 499−515

bluish-white and yellowish-green OLED devices have been fabricated. The chemosensing enactment of the m-CF_3PTPI luminophores was confirmed by the lifetime and TD-DFT study. The mechanisms were proposed by the experimental and theoretical study. Compared with other nitroaromatics, PA shows more quenching efficiency and the detection limits of m-CF_3PTPI luminophores are in the range of 104−249 ppb.

■ ASSOCIATED CONTENT

Supporting Information

The Supporting Information is available free of charge at https://pubs.acs.org/doi/10.1021/acs.jpcc.2c05220.

NMR spectra, mass spectra, chemosensor data including photoluminescence spectra, lifetime measurements, and tables and images of DFT analysis (PDF)

■ AUTHOR INFORMATION

Corresponding Author

Sivakumar Vaidyanathan − *Department of Chemistry, National Institute of Technology Rourkela, Rourkela 769 008 Odisha, India; Department of Chemistry, Indian Institute of Technology, Sangareddy 502285 Telangana, India;* orcid.org/0000-0002-2104-2627; Email: vsiva@chy.iith.ac.in

Authors

Sandhya Rani Nayak − *Department of Chemistry, National Institute of Technology Rourkela, Rourkela 769 008 Odisha, India*

Shahnawaz − *Department of Materials Science and Engineering, National Tsing Hua University, Hsinchu 30013, Taiwan ROC*

Iram Siddiqui − *Department of Materials Science and Engineering, National Tsing Hua University, Hsinchu 30013, Taiwan ROC*

Jwo-Huei Jou − *Department of Materials Science and Engineering, National Tsing Hua University, Hsinchu 30013, Taiwan ROC*

Sabita Patel − *Department of Chemistry, National Institute of Technology Rourkela, Rourkela 769 008 Odisha, India*

Complete contact information is available at: https://pubs.acs.org/10.1021/acs.jpcc.2c05220

Notes

The authors declare no competing financial interest.

■ ACKNOWLEDGMENTS

S.V. acknowledges SERB, Department of Science and Technology (DST), India (EMR/2016/002462, CRG/2021/000494) for financial support. The authors also thank Miss Ting-Yin Cheng at the Instrumentation Centre of National Tsing Hua University for the thermogravimetric analysis (TGA).

■ REFERENCES

(1) Narayanaswamy, K.; Venkateswararao, A.; Nagarjuna, P.; Bishnoi, S.; Gupta, V.; Chand, S.; Singh, S. P. An Organic Dyad Composed of Diathiafulvalene-Functionalized Diketopyrrolopyrrole−Fullerene for Single-Component High-Efficiency Organic Solar Cells. *Angew. Chemie Int. Ed.* **2016**, *55*, 12334−12337.

(2) Devesing Girase, J.; Rani Nayak, S.; Tagare, J.; Shahnawaz; Ram Nagar, M.; Jou, J.-H.; Vaidyanathan, S. Solution-Processed Deep-Blue (Y∼0.06) Fluorophores Based on Triphenylamine-Imidazole (Donor-Acceptor) for OLEDs: Computational and Experimental Exploration. *J. Inf. Disp.* **2021**, 1−15.

(3) Adil, L. R.; Iyer, P. K. Effects of Incorporating Regioisomers and Flexible Rotors to Direct Aggregation Induced Emission to Achieve Stimuli-Responsive Luminogens, Security Inks and Chemical Warfare Agent Sensors. *Chem. Commun.* **2020**, *56*, 7633−7636.

(4) Shih, P.-I.; Tseng, Y.-H.; Wu, F.-I.; Dixit, A. K.; Shu, C.-F. Stable and Efficient White Electroluminescent Devices Based on a Single Emitting Layer of Polymer Blends. *Adv. Funct. Mater.* **2006**, *16*, 1582−1589.

(5) Kajjam, A. B.; Vaidyanathan, S. Structural Mimics of Phenyl Pyridine (Ppy) − Substituted, Phosphorescent Cyclometalated Homo and Heteroleptic Iridium(III) Complexes for Organic Light Emitting Diodes − An Overview. *Chem. Rec.* **2018**, *18*, 293−349.

(6) Lee, J.-H.; Zhu, X.; Lin, Y.-H.; Kit Choi, W.; Lin, T.-C.; Hsu, S.-C.; Lin, H.-Y.; Wu, S.-T. High Ambient-Contrast-Ratio Display Using Tandem Reflective Liquid Crystal Display and Organic Light-Emitting Device. *Opt. Express* **2005**, *13*, 9431−9438.

(7) Hung, L. S.; Chen, C. H. Recent Progress of Molecular Organic Electroluminescent Materials and Devices. *Mater. Sci. Eng. R Reports* **2002**, *39*, 143−222.

(8) Goushi, K.; Yoshida, K.; Sato, K.; Adachi, C. Organic Light-Emitting Diodes Employing Efficient Reverse Intersystem Crossing for Triplet-to-Singlet State Conversion. *Nat. Photonics* **2012**, *6*, 253−258.

(9) Zhu, M.; Yang, C. Blue Fluorescent Emitters: Design Tactics and Applications in Organic Light-Emitting Diodes. *Chem. Soc. Rev.* **2013**, *42*, 4963−4976.

(10) Cleave, V.; Yahioglu, G.; Le Barny, P.; Friend, R. H.; Tessler, N. Harvesting Singlet and Triplet Energy in Polymer LEDs. *Adv. Mater.* **1999**, *11*, 285−288.

(11) Adachi, C.; Kwong, R. C.; Djurovich, P.; Adamovich, V.; Baldo, M. A.; Thompson, M. E.; Forrest, S. R. Endothermic Energy Transfer: A Mechanism for Generating Very Efficient High-Energy Phosphorescent Emission in Organic Materials. *Appl. Phys. Lett.* **2001**, *79*, 2082−2084.

(12) Xiao, L.; Chen, Z.; Qu, B.; Luo, J.; Kong, S.; Gong, Q.; Kido, J. Recent Progresses on Materials for Electrophosphorescent Organic Light-Emitting Devices. *Adv. Mater.* **2011**, *23*, 926−952.

(13) Wu, Z.; Xiong, Y.; Zou, J.; Wang, L.; Liu, J.; Chen, Q.; Yang, W.; Peng, J.; Cao, Y. High-Triplet-Energy Poly(9,9′-Bis(2-Ethylhexyl)-3,6-Fluorene) as Host for Blue and Green Phosphorescent Complexes. *Adv. Mater.* **2008**, *20*, 2359−2364.

(14) Girase, J. D.; Kajjam, A. B.; Dubey, D. K.; Kesavan, K. K.; Jou, J.-H.; Vaidyanathan, S. Unipolar 1-Phenylimidazo[1,5-a]Pyridine: A New Class of Ultra-Bright Sky Blue Emitters for Solution-Processed Organic Light Emitting Diodes. *New J. Chem.* **2022**, 16717.

(15) Usman, K.; Islam, A.; Ullah Shah, S. H.; Javaid, K.; Amin, A.; Mustafa, Z.; Wattoo, A. G.; Abbas, N.; Ge, Z. Fluorescent Pyrene-Imidazole Material for Deep-Blue Organic Light-Emitting Devices. *Opt. Mater. (Amst).* **2021**, *121*, No. 111582.

(16) Kajjam, A. B.; Dubey, D. K.; Kumar Yadav, R. A.; Jou, J.-H.; Sivakumar, V. Tetraphenylimidazole-Based Luminophores for Explosive Chemosensors and OLEDs: Experimental and Theoretical Investigation. *Mater. Today Chem.* **2019**, *14*, No. 100201.

(17) Tagare, J.; Dubey, D. K.; Yadav, R. A. K.; Jou, J.-H.; Vaidyanathan, S. Triphenylamine-Imidazole-Based Luminophores for Deep-Blue Organic Light-Emitting Diodes: Experimental and Theoretical Investigations. *Mater. Adv.* **2020**, *1*, 666−679.

(18) Li, C.; Wei, J.; Song, X.; Ye, K.; Zhang, H.; Zhang, J.; Wang, Y. Non-Doped Luminescent Material Based Organic Light-Emitting Devices Displaying High Brightness under Very Low Driving Voltage. *J. Mater. Chem. C* **2016**, *4*, 7013−7019.

(19) Jadhav, T.; Choi, J. M.; Lee, J. Y.; Dhokale, B.; Misra, R. Non-Doped Blue Organic Light Emitting Devices Based on Tetraphenylethylene-π-Imidazole Derivatives. *Org. Electron.* **2016**, *37*, 448−452.

(20) Ge, Z.; Hayakawa, T.; Ando, S.; Ueda, M.; Akiike, T.; Miyamoto, H.; Kajita, T.; Kakimoto, M. Spin-Coated Highly Efficient Phosphorescent Organic Light-Emitting Diodes Based on Bipolar

Triphenylamine-Benzimidazole Derivatives. *Adv. Funct. Mater.* **2008**, *18*, 584−590.
(21) Béreau, V.; Duhayon, C.; Sutter, J.-P. Supramolecular Control over Recognition and Efficient Detection of Picric Acid. *Chem. Commun.* **2014**, *50*, 12061−12064.
(22) Wang, X.; Bian, J.; Xu, L.; Wang, H.; Feng, S. Thiophene Functionalized Silicon-Containing Aggregation-Induced Emission Enhancement Materials: Applications as Fluorescent Probes for the Detection of Nitroaromatic Explosives in Aqueous-Based Solutions. *Phys. Chem. Chem. Phys.* **2015**, *17*, 32472−32478.
(23) Zhang, M.; Xue, S.; Dong, W.; Wang, Q.; Fei, T.; Gu, C.; Ma, Y. Highly-Efficient Solution-Processed OLEDs Based on New Bipolar Emitters. *Chem. Commun.* **2010**, *46*, 3923−3925.
(24) Kajjam, A. B.; Singh, K.; Tej, R. V. V.; Vaidyanathan, S. Carbazole−Acenaphthene (Donor−Acceptor)-Based Luminophores for Picric Acid Detection: A Combined Experimental and Theoretical Study. *Mater. Adv.* **2021**, *2*, 5236−5247.
(25) Murali, M. G.; Rao, A. D.; Ramamurthy, P. C. New Low Band Gap 2-(4-(Trifluoromethyl)Phenyl)-1H-Benzo[d]Imidazole and Benzo[1,2-c;4,5-C′]Bis[1,2,5]Thiadiazole Based Conjugated Polymers for Organic Photovoltaics. *RSC Adv.* **2014**, *4*, 44902−44910.
(26) Huang, Y.; Huo, L.; Zhang, S.; Guo, X.; Han, C. C.; Li, Y.; Hou, J. Sulfonyl: A New Application of Electron-Withdrawing Substituent in Highly Efficient Photovoltaic Polymer. *Chem. Commun.* **2011**, *47*, 8904−8906.
(27) Shim, J. Y.; Kim, T.; Kim, J.; Kim, J.; Kim, I.; Kim, J. Y.; Suh, H. Trifluoromethyl Benzimidazole-Based Conjugated Polymers with Deep HOMO Levels for Organic Photovoltaics. *Synth. Met.* **2015**, *205*, 112−120.
(28) Casey, A.; Dimitrov, S. D.; Shakya-Tuladhar, P.; Fei, Z.; Nguyen, M.; Han, Y.; Anthopoulos, T. D.; Durrant, J. R.; Heeney, M. Effect of Systematically Tuning Conjugated Donor Polymer Lowest Unoccupied Molecular Orbital Levels via Cyano Substitution on Organic Photovoltaic Device Performance. *Chem. Mater.* **2016**, *28*, 5110−5120.
(29) Qin, A.; Tang, L.; Lam, J. W. Y.; Jim, C. K. W.; Yu, Y.; Zhao, H.; Sun, J.; Tang, B. Z. Metal-Free Click Polymerization: Synthesis and Photonic Properties of Poly(Aroyltriazole)S. *Adv. Funct. Mater.* **2009**, *19*, 1891−1900.
(30) Hwang, S.; Lee, J. H.; Park, C.; Lee, H.; Kim, C.; Park, C.; Lee, M.-H.; Lee, W.; Park, J.; Kim, K.; et al. A Highly Efficient Organic Sensitizer for Dye-Sensitized Solar Cells. *Chem. Commun.* **2007**, *46*, 4887−4889.
(31) Fitri, A.; Benjelloun, A. T.; Benzakour, M.; Mcharfi, M.; Hamidi, M.; Bouachrine, M. Theoretical Design of Thiazolothiazole-Based Organic Dyes with Different Electron Donors for Dye-Sensitized Solar Cells. *Spectrochim. Acta Part A Mol. Biomol. Spectrosc.* **2014**, *132*, 232−238.
(32) Kajjam, A. B.; Kumar, P. S. V.; Subramanian, V.; Vaidyanathan, S. Triphenylamine Based Yellowish-Orange Light Emitting Organic Dyes (Donor−π−Acceptor) for Hybrid WLEDs and OLEDs: Synthesis, Characterization and Theoretical Study. *Phys. Chem. Chem. Phys.* **2018**, *20*, 4490−4501.
(33) Strohriegl, P.; Grazulevicius, J. V. Charge-Transporting Molecular Glasses. *Adv. Mater.* **2002**, *14*, 1439−1452.
(34) Wagner, D.; Hoffmann, S. T.; Heinemeyer, U.; Münster, I.; Köhler, A.; Strohriegl, P. Triazine Based Bipolar Host Materials for Blue Phosphorescent OLEDs. *Chem. Mater.* **2013**, *25*, 3758−3765.
(35) Tagare, J.; Boddula, R.; Sudheendran, S. S.; Dubey, D. K.; Jou, J.-H.; Patel, S.; Vaidyanathan, S. Efficient near Ultraviolet Emissive (CIEy < 0.06) Organic Light-Emitting Diodes Based on Phenanthroimidazole−Alkyl Spacer−Carbazole Fluorophores: Experimental and Theoretical Investigation. *J. Mater. Chem. C* **2020**, *8*, 16834−16844.
(36) Chen, W.-C.; Lee, C.-S. The Development of Phenanthroimidazole Derivatives in Blue-Emitting Organic Electroluminescence. *Sci. Adv. Mater.* **2015**, *7*, 2193−2205.
(37) Zhou, Y.; Zhang, M.; Ye, J.; Liu, H.; Wang, K.; Yuan, Y.; Du, Y.-Q.; Zhang, C.; Zheng, C.-J.; Zhang, X.-H. Efficient Solution-Processed Red Organic Light-Emitting Diode Based on an Electron-Donating Building Block of Pyrrolo[3,2-b]Pyrrole. *Org. Electron.* **2019**, *65*, 110−115.
(38) Wu, C.-L.; Chang, C.-H.; Chang, Y.-T.; Chen, C.-T.; Chen, C.-T.; Su, C.-J. High Efficiency Non-Dopant Blue Organic Light-Emitting Diodes Based on Anthracene-Based Fluorophores with Molecular Design of Charge Transport and Red-Shifted Emission Proof. *J. Mater. Chem. C* **2014**, *2*, 7188−7200.
(39) Huang, J.; Sun, N.; Dong, Y.; Tang, R.; Lu, P.; Cai, P.; Li, Q.; Ma, D.; Qin, J.; Li, Z. Similar or Totally Different: The Control of Conjugation Degree through Minor Structural Modifications, and Deep-Blue Aggregation-Induced Emission Luminogens for Non-Doped OLEDs. *Adv. Funct. Mater.* **2013**, *23*, 2329−2337.
(40) Chen, S.; Lian, J.; Wang, W.; Jiang, Y.; Wang, X.; Chen, S.; Zeng, P.; Peng, Z. Efficient Deep Blue Electroluminescence with CIEy ∈ (0.05−0.07) from Phenanthroimidazole−Acridine Derivative Hybrid Fluorophores. *J. Mater. Chem. C* **2018**, *6*, 9363−9373.
(41) Zhao, N.; Li, M.; Yan, Y.; Lam, J. W. Y.; Zhang, Y. L.; Zhao, Y. S.; Wong, K. S.; Tang, B. Z. A Tetraphenylethene-Substituted Pyridinium Salt with Multiple Functionalities: Synthesis, Stimuli-Responsive Emission, Optical Waveguide and Specific Mitochondrion Imaging. *J. Mater. Chem. C* **2013**, *1*, 4640−4646.
(42) Tagare, J.; Boddula, R.; Yadav, R. A. K.; Dubey, D. K.; Jou, J.-H.; Patel, S.; Vaidyanathan, S. Novel Imidazole-Alkyl Spacer-Carbazole Based Fluorophores for Deep-Blue Organic Light Emitting Diodes: Experimental and Theoretical Investigation. *Dyes Pigm.* **2021**, *185*, No. 108853.
(43) Jiang, W.; Ge, Z.; Cai, P.; Huang, B.; Dai, Y.; Sun, Y.; Qiao, J.; Wang, L.; Duan, L.; Qiu, Y. Star-Shaped Dendritic Hosts Based on Carbazole Moieties for Highly Efficient Blue Phosphorescent OLEDs. *J. Mater. Chem.* **2012**, *22*, 12016−12022.
(44) Li, W.; Li, J.; Liu, D.; Wang, F.; Zhang, S. Bipolar Host Materials for High-Efficiency Blue Phosphorescent and Delayed-Fluorescence OLEDs. *J. Mater. Chem. C* **2015**, *3*, 12529−12538.
(45) Li, W.; Li, J.; Wang, F.; Gao, Z.; Zhang, S. Universal Host Materials for High-Efficiency Phosphorescent and Delayed-Fluorescence OLEDs. *ACS Appl. Mater. Interfaces* **2015**, *7*, 26206−26216.
(46) de Leeuw, D. M.; Simenon, M. M. J.; Brown, A. R.; Einerhand, R. E. F. Stability of N-Type Doped Conducting Polymers and Consequences for Polymeric Microelectronic Devices. *Synth. Met.* **1997**, *87*, 53−59.
(47) Tao, Y.; Wang, Q.; Ao, L.; Zhong, C.; Qin, J.; Yang, C.; Ma, D. Molecular Design of Host Materials Based on Triphenylamine/Oxadiazole Hybrids for Excellent Deep-Red Phosphorescent Organic Light-Emitting Diodes. *J. Mater. Chem.* **2010**, *20*, 1759−1765.
(48) Yuan, W. Z.; Hu, R.; Lam, J. W. Y.; Xie, N.; Jim, C. K. W.; Tang, B. Z. Conjugated Hyperbranched Poly(Aryleneethynylene)s: Synthesis, Photophysical Properties, Superquenching by Explosive, Photopatternability, and Tunable High Refractive Indices. *Chem. − A Eur. J.* **2012**, *18*, 2847−2856.
(49) An, Z.-F.; Zheng, C.; Chen, R.-F.; Yin, J.; Xiao, J.-J.; Shi, H.-F.; Tao, Y.; Qian, Y.; Huang, W. Exceptional Blueshifted and Enhanced Aggregation-Induced Emission of Conjugated Asymmetric Triazines and Their Applications in Superamplified Detection of Explosives. *Chem. − A Eur. J.* **2012**, *18*, 15655−15661.
(50) Thomas, S. W.; Joly, G. D.; Swager, T. M. Chemical Sensors Based on Amplifying Fluorescent Conjugated Polymers. *Chem. Rev.* **2007**, *107*, 1339−1386.
(51) Lin, J.-J.; Liao, W.-S.; Huang, H.-J.; Wu, F.-I.; Cheng, C.-H. A Highly Efficient Host/Dopant Combination for Blue Organic Electrophosphorescence Devices. *Adv. Funct. Mater.* **2008**, *18*, 485−491.
(52) Chen, Y.-C.; Huang, G.-S.; Hsiao, C.-C.; Chen, S.-A. High Triplet Energy Polymer as Host for Electrophosphorescence with High Efficiency. *J. Am. Chem. Soc.* **2006**, *128*, 8549−8558.
(53) Santra, D. C.; Bera, M. K.; Sukul, P. K.; Malik, S. Charge-Transfer-Induced Fluorescence Quenching of Anthracene Derivatives and Selective Detection of Picric Acid. *Chem. − A Eur. J.* **2016**, *22*, 2012−2019.

https://doi.org/10.1021/acs.jpcc.2c05220
J. Phys. Chem. C 2023, 127, 499−515

(54) Pandith, A.; Kumar, A.; Lee, J.-Y.; Kim, H.-S. 9-Anthracenecarboxamide Fluorescent Probes for Selective Discrimination of Picric Acid from Mono- and Di-Nitrophenols in Ethanol. *Tetrahedron Lett.* **2015**, *56*, 7094−7099.
(55) Shanmugaraju, S.; Jadhav, H.; Patil, Y. P.; Mukherjee, P. S. Self-Assembly of an Octanuclear Platinum(II) Tetragonal Prism from a New PtII4 Organometallic Star-Shaped Acceptor and Its Nitroaromatic Sensing Study. *Inorg. Chem.* **2012**, *51*, 13072−13074.
(56) Venkatramaiah, N.; Kumar, S.; Patil, S. Femtogram Detection of Explosive Nitroaromatics: Fluoranthene-Based Fluorescent Chemosensors. *Chem. − A Eur. J.* **2012**, *18*, 14745−14751.
(57) Chen, S.-H.; Jiang, K.; Lin, J.-Y.; Yang, K.; Cao, X.-Y.; Luo, X.-Y.; Wang, Z.-Y. Rational Design and Synthesis of Y-Shaped Fluorophores with Multifarious Emission Properties and Their Application in the Sensitive Detection of PA. *J. Mater. Chem. C* **2020**, *8*, 8257−8267.

https://doi.org/10.1021/acs.jpcc.2c05220
J. Phys. Chem. C 2023, 127, 499−515